SDL-2-588

Semi-Annual Progress Report No. 2

NASA Grant NsG-588

Theoretical and Experimental Studies of Radiation-Induced Damage to Semiconductor Surfaces and the Effects of this Damage on Semiconductor Device Performance

1 September 1964 through 28 February 1965

Prepared by

Semiconductor Device Laboratory

Department of Electrical Engineering
North Carolina State
of the
University of North Carolina
at
Raleigh, North Carolina

SDL-2-588

Semi-Annual Progress Report No. 2

NASA Grant NsG-588

Theoretical and Experimental Studies of Radiation-Induced Damage to Semiconductor Surfaces and the Effects of this Damage on Semiconductor Device Performance

1 September 1964 through 28 February 1965

Prepared by

Semiconductor Device Laboratory

Department of Electrical Engineering
North Carolina State
of the
University of North Carolina
at
Raleigh, North Carolina

ABSTRACT

21354

During the period 1 September 1964 through 28 February 1965, this project expanded into three distinct areas of research. Work on the gamma irradiation studies of silicon surfaces progressed at a normal pace and data on polished surfaces are included in this report.

A study was initiated to determine the variation in the surface potential and the surface state charge distribution in the oxide passivated materials using an insulated gate field effect transister structure.

During the latter part of this period, analytical studies of device performance with the inclusion of surface parameters was initiated. Some preliminary results are included for the one-dimensional planar solar cell.

This report concludes with a projection of plans for the next six-month period.

I. Filament Studies

A. Introduction

As indicated in SDL report # 1-588, the Photo-electro magnetic (P.E.M.) effect allows direct measurement of the bulk lifetime, τ_b, and the surface recombination velocity, S, under certain assumptions in the analysis of the device (filament) problem. However, these assumptions are too severe to allow accurate calculations of these parameters under most practical experimental conditions. (SDL report # 1-588, pp. 12-13). Also, the illumination intensity required to obtain these parameters is of such a magnitude that no reasonable correlation between data obtained by the P.E.M. effect and that obtained by the method of photoconductive decay (P.C.D.) can be expected.[1]

Due to these limitations on the P.E.M. effect, values of and S will be obtained using the method of P.C.D. as described in SDL report # 1-588, pp. 3-5 with the experimental setup shown on page 9 of that report.

B. Experimental Technique

To measure τ_b by the method of PCD, a standard bulk sample is required. The dimensions of this sample were chosen as .5cm x .5cm x 1.5cm since a filament with a square cross sectional area facilitates easier data reduction. Three bulk samples of these dimensions can be obtained from one .5cm slice from a 1" diam. ingot of silicon, the slice being cut with a diamond saw perpendicular to the longitudinal axis of the ingot. After the three samples are cut, they are lapped on all sides with #100 grit until any

dislocations caused by the diamond saw are removed. Then they are boiled in TCE for approximately 5 minutes, dried, and placed in an electroless nickel plating solution at approximately 90°C for 10 min. After this nickel plating, the four sides are lapped again until all the nickel plating is removed, leaving the ends of the samples plated for ohmic contacts. The bulk samples are then ready for measurements. The lapped sides provide surfaces such that $S \rightarrow \infty$, and thus τ_s approaches a constant value which is a function of the sample dimensions and the minority carrier (ambi-polar) diffusivity. Then τ_b can be calculated from

$$1) \quad 1/\tau_b = 1/\tau_f - 1/\tau_s$$

where τ_f is the value measured by the PCD method.

The surface recombination velocity for other specimens can be determined if τ_b and τ_f are known, since $1/\tau_s$ can then be calculated from (1) and use of the curves shown on pp. 18 of SDL report #1-588. These curves give the value of S as a function of $1/\tau_s$ and the sample dimensions. For this measurement, samples with dimensions of .02cm x .5cm x 1.5cm were chosen. The samples are lapped with #800 grit until saw dislocations are removed. They are then boiled in TCE for 5 minutes and nickel plated in the same manner as the bulk samples. The ends are then coated with apiezon wax, and the wax allowed to dry for approximately 24 hours. The samples are then etched in a 25ml. mixture of 98% HNO_3 and 2% HF for 20 min. with 2-4 drops of HF added every five minutes. This etching removes the nickel plating from the sides and chemically polishes the samples to complete the surface preparation. The apiezon wax is then removed from the ends with TCE and the samples are ready for measurements.

In order for the values of S to be meaningful, the values of τ_b for the thin filaments must be accurately known. It has been observed that the values of τ_b vary considerably with radial distance in the silicon ingots used, and thus the orientation of the slices used to make the thin filaments and bulk samples can not be arbitrary. To facilitate the correlation of the bulk lifetime of the thin filaments to the bulk samples, a standard procedure has been devised to make samples.

First, the ingot is mounted on a piece of ceramic tile for use in the diamond saw. The ingot is then cut along a chord of the circular cross section parallel to the longitudinal axis of the ingot. This provides a reference edge and all samples are cut with their longest dimension parallel to this edge.

To correlate the values of bulk lifetime for the thin filament and the bulk samples, two slices .5cm thick are cut from the ingot. Both slices are then mounted, one upon the other, on a piece of ceramic tile. The bulk samples are then cut from this configuration, with caution taken to differentiate between corresponding samples from each slice. Thus six bulk samples result from the two slices, and the lifetime of each sample is measured. If the values of lifetime of corresponding samples are within 10% of each other, then one of the corresponding samples is cut into three thin filaments. For each bulk sample with a given bulk lifetime, there then results three thin filaments with the same bulk lifetime (to within 10%).

C. N-Type Silicon

To begin the irradiation experiments, 100 Ω cm n-type silicon was chosen as the first material to examine. Two bulk

samples and five thin filaments were made, all lapped with #100 grit on the sides. Two of the thin filaments were then etched for 15 min. each in 95% HNO_3 and 5% HF. These samples were to be studied in order to determine the order of magnitude changes in bulk lifetime and surface recombination velocity as a function of radiation dosage, and thus no strict procedure for surface preparation and thin filament dimensions was adhered to. Also, from the first report, it was realized that the ambient under which the irradiations were carried out is an important factor, and thus different ambients were to be used with each irradiation. Graphs No. 1, 2, and 3 show the results of low energy gamma irradiation on bulk lifetime and surface recombination velocity, normalized to the pre-irradiation valves.

The first irradiation was carried out in a forming gas atmosphere (95% N_2, 5% H_2). There is a marked reduction of the value of bulk lifetime for the two bulk samples 1NA58-1 and 1NA58-2, the change being at least two orders of magnitude for both samples. There is likewise a reduction of the value of surface recombination velocity for the five thin filaments, the percentage change being greater for the filaments that were not etched. Also, the pre-irradiation values of S for these samples were at least a factor of 2 greater than those for the etched filaments.

The second irradiation was carried out in an argon atmosphere, and again the bulk lifetime decreased. However, the percentage change was much less, being on the order of 25% for both samples. An examination of the values of surface recombination velocity

GRAPH-1

O - SAMPLE 1NA58-1 $\tau_{60} = 339\mu s$
X - SAMPLE 1NA58-2 $\tau_{60} = 546\mu s$
IRRADIATION RATE = 0.25 MEGARAD/HR.

#1 - FORMING GAS AMBIENT
#2 - ARGON AMBIENT
#3 - ATMOSPHERIC AMBIENT
*3 - PREDICTED VALUE IF NON-OXIDIZING AMBIENT HAD BEEN MAINTAINED

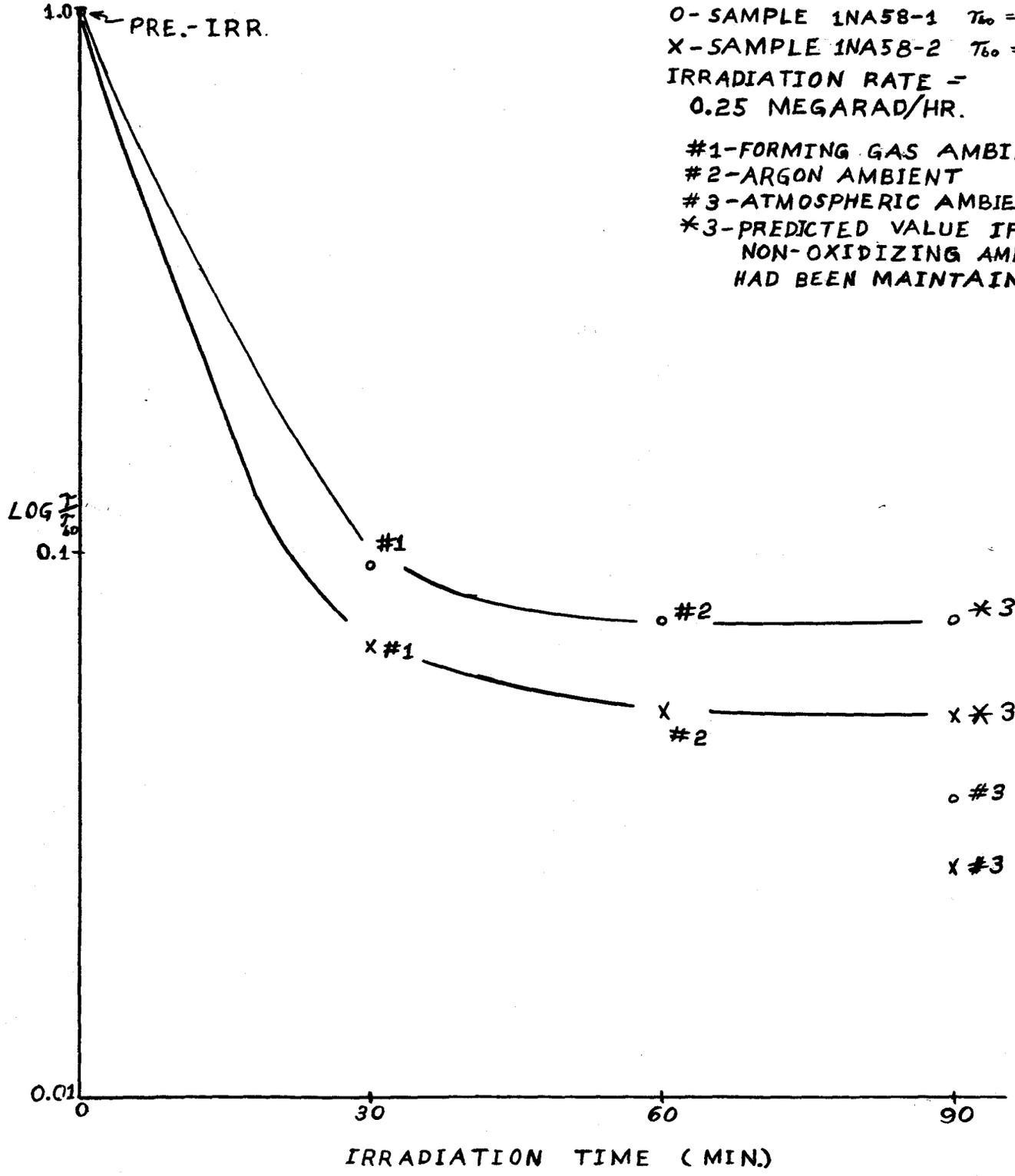

GRAPH-2

CORRESPOND TO BULK SAMPLE - 1NA58-1
IRRADIATION RATE = 0.25 MEGARAD/HR.

O - SAMPLE 1NA 3/8 8-1 (POL.) S_o = 2595 cm/sec
X - SAMPLE 1NA 3/8 8-2 S_o = 6620 cm/sec
Δ - SAMPLE 1NA 3/8 8-3 S_o = 5930 cm/sec

#1 - FORMING GAS AMBIENT
#2 - ARGON AMBIENT
#3 - ATMOSPHERIC AMBIENT
*3 - PREDICTED VALUE IF NON-OXIDIZING AMBIENT HAD BEEN MAINTAINED

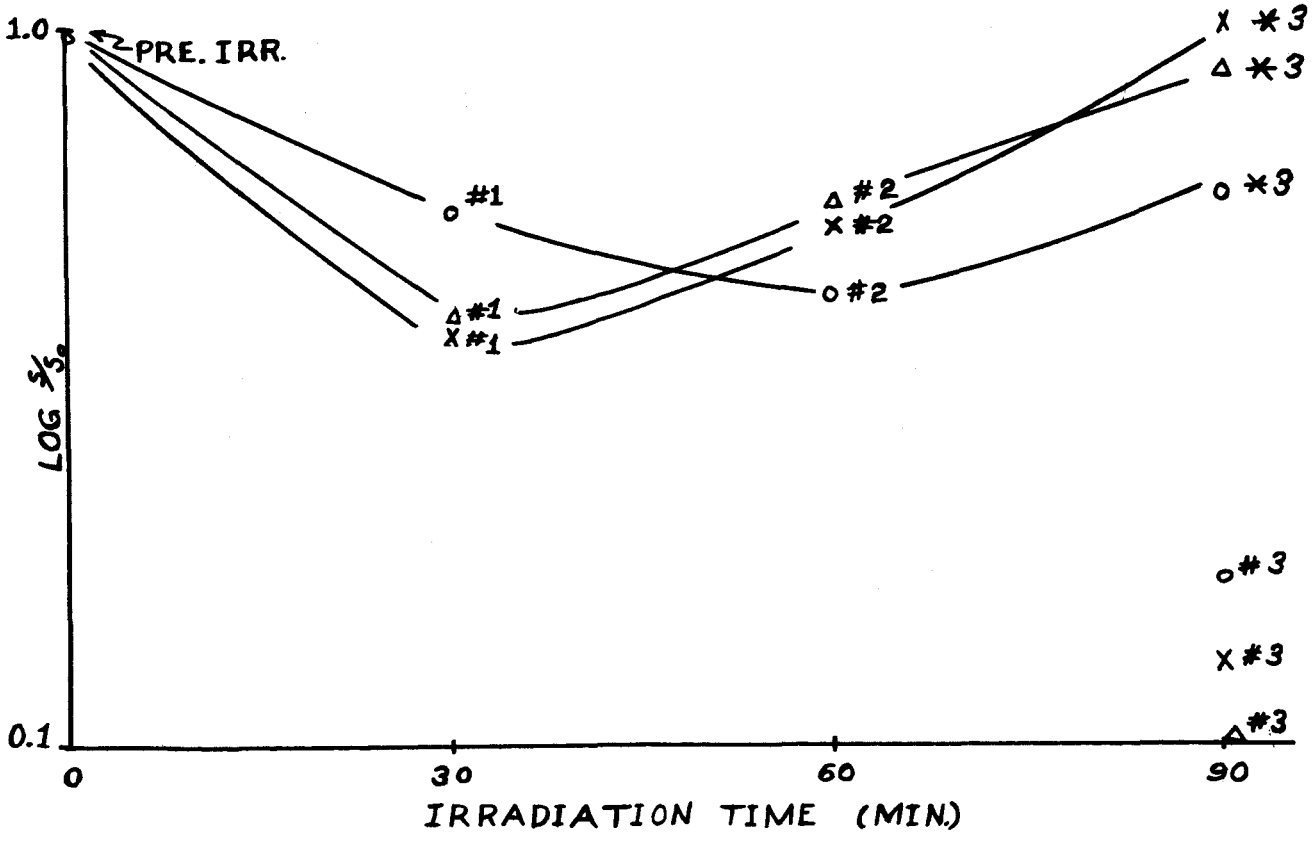

GRAPH-3

CORRESPONDING TO BULK SAMPLE 1NA58-2

IRRADIATION RATE = 0.25 MEGARAD./HR.

O - SAMPLE 1NA 3/8 B-4 (POL.) S_o = 2370 cm/sec

X - SAMPLE 1NA 3/8 B-6 S_o = > 10^4 cm/sec

#1 - FORMING GAS AMBIENT

#2 - ARGON AMBIENT

#3 - ATMOSPHERIC AMBIENT

*3 - PREDICTED VALUE IF NON-OXIDIZING AMBIENT HAD BEEN MAINTAINED

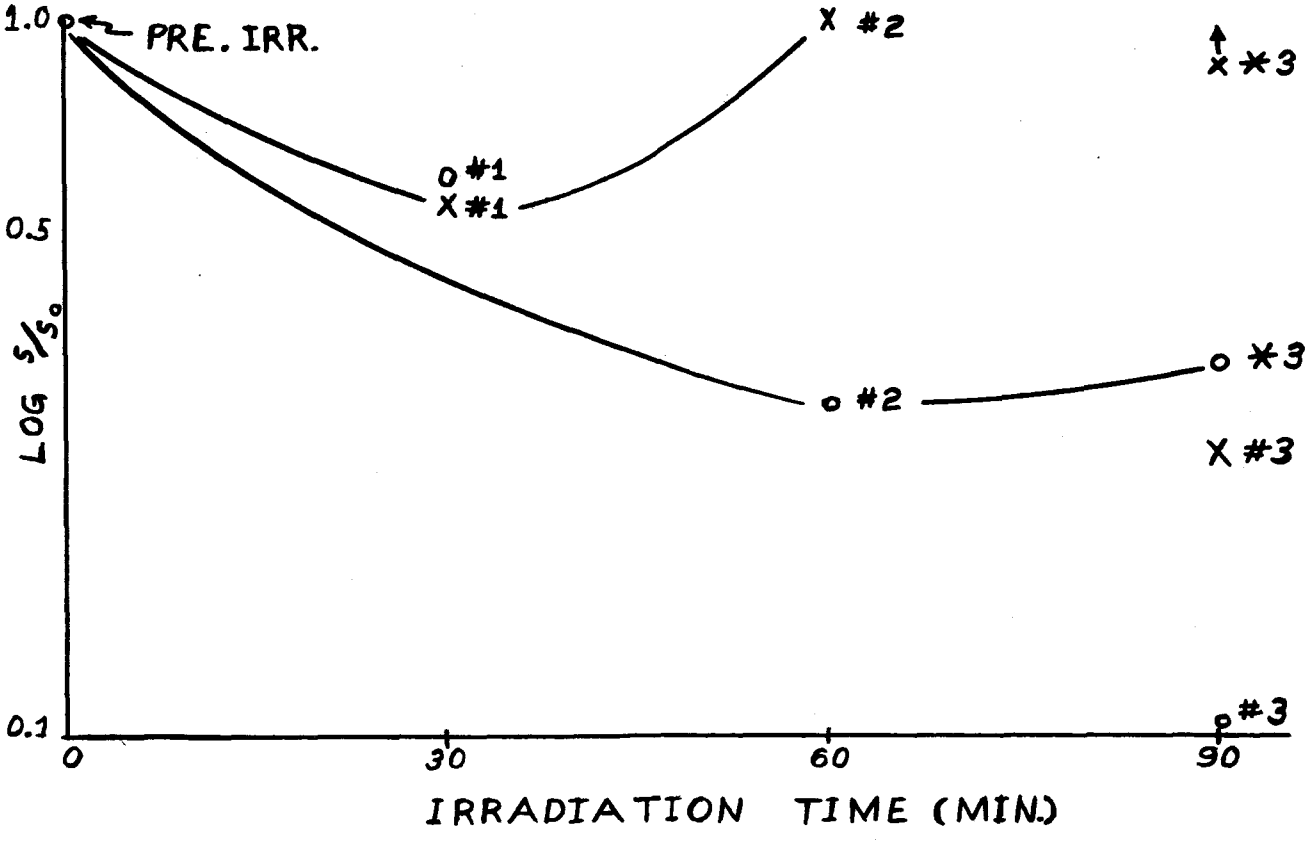

showed that S continued to decrease for the etched samples, but increased for the filaments with "sand blasted" surfaces.

The third irradiation was carried out in air, and the bulk lifetime continued to decrease. The percentage change from the 2nd irradiation was greater than 50% for both samples. Also, the value of surface recombination velocity decreased for each of the thin filaments, the total change being greater than 75% in all cases. This again illustrates the adverse effect of irradiation in a non-oxidizing atmosphere for n-type material.

Due to the fact that samples 1NA 3/8 5 - 2, 3, and 6 showed a marked increase in surface recombination velocity between the first and second irradiations, and the fact that the irradiation carried out in air deviated drastically from the rest of the data, an extrapolation procedure was carried out in hopes of predicating results if the third irradiation had been carried out in a non-oxidizing atmosphere. First of all, the points on graph # 1 were plotted, and then a smooth curve was drawn through points #1 and # 2. This curve was extended, and a corrected value of bulk lifetime was obtained as shown in the graph. These values of were then used to correct the values of S in graphs # 2 and 3. These corrected values showed an increase from the value for irradiation # 2 in all cases. With these preliminary results, it was decided to conduct another experiment on a new set of samples, while maintaining a non-oxidizing atmosphere during each irradiation. Argon gas was chosen for this purpose.

A set of three bulk samples and nine thin filaments were made and bulk lifetime and surface recombination velocity measured as

a function of irradiation dosage. Graphs 4, 5, 6, 7, and 8 show the results of these measurements carried out in an argon atmosphere. In every case, the bulk lifetime decreases drastically with initial irradiation, and then continues to decrease slowly with each additional irradiation. On the other hand, a minimum in surface recombination velocity exists for each filament. That is, surface recombination velocity decreases with initial irradiation, and then increases with additional irradiation. There is one exception, which can be seen in graph #7. These three samples, all having the same bulk lifetime, show a decrease in S after a fourth irradiation. However, in order to make the measurements of filament lifetime on these samples, the intensity of light used for carrier injection had to be reduced in order to eliminate the characteristic "hump" in the decay curve, noted after several irradiations for n-type samples in the first report. It is well known that both the bulk and filament lifetimes are a function of illumination intensity when light is used to inject excess carriers into a semiconductor. Hence, it can be concluded that this point is not meaningful since the experimental conditions have been changed.[1] A small amount of foresight is all that is needed to eliminate this apparent problem.

In computing the value of S it has been assumed that the ambi-polar diffusivity does not vary with irradiation. To verify that any variations would not change the results, Hall Effect measurements were carried out, the actual diffusivity calculated, and the value of S recalculated. The following table illustrates

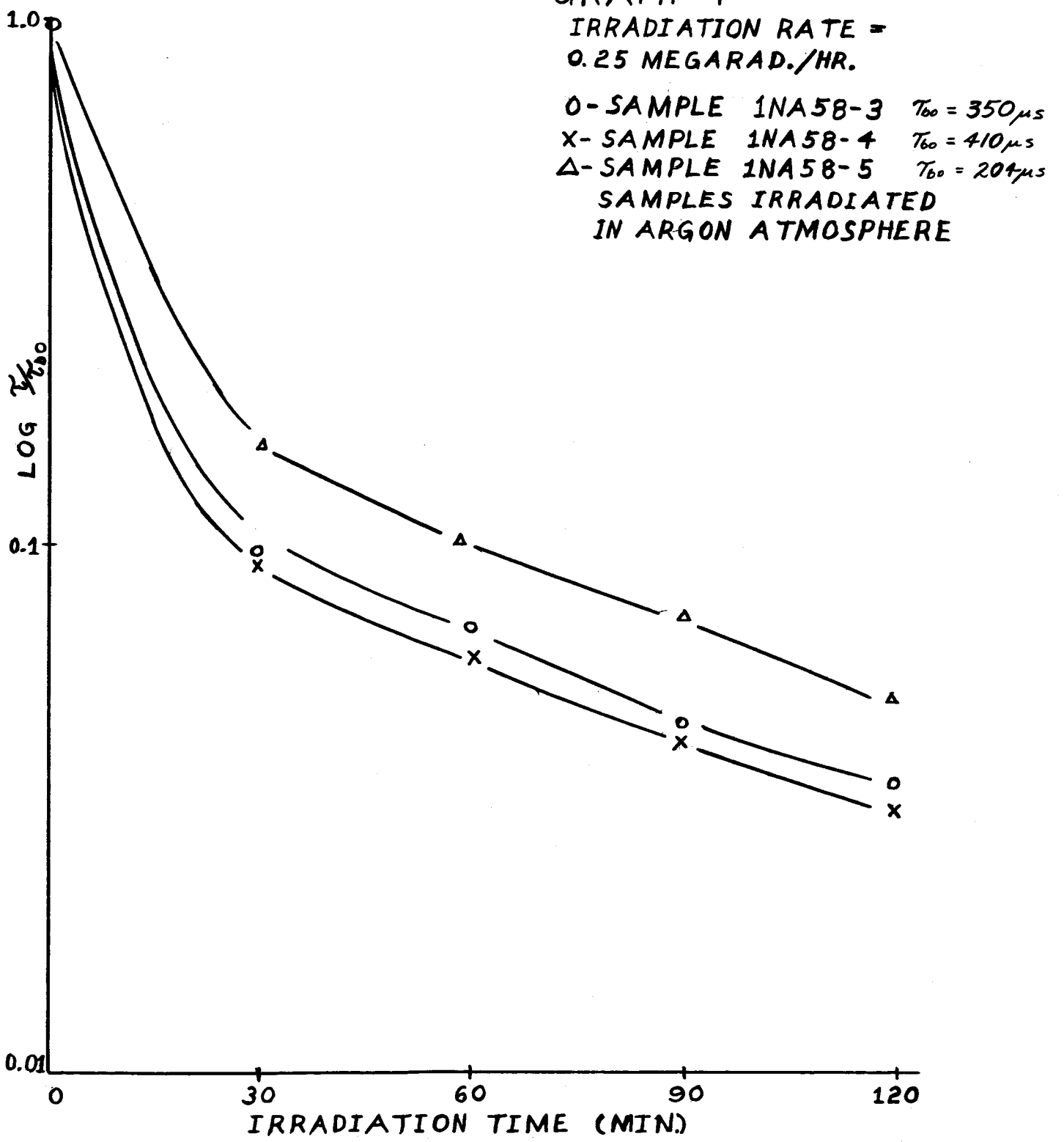
GRAPH-4
IRRADIATION RATE =
0.25 MEGARAD./HR.
O - SAMPLE 1NA58-3 $\tau_{60} = 350\mu s$
X - SAMPLE 1NA58-4 $\tau_{60} = 410\mu s$
Δ - SAMPLE 1NA58-5 $\tau_{60} = 204\mu s$
SAMPLES IRRADIATED
IN ARGON ATMOSPHERE
1.0
0.1
0.01
LOG τ/τ_{60}
0
30
60
90
120
IRRADIATION TIME (MIN.)

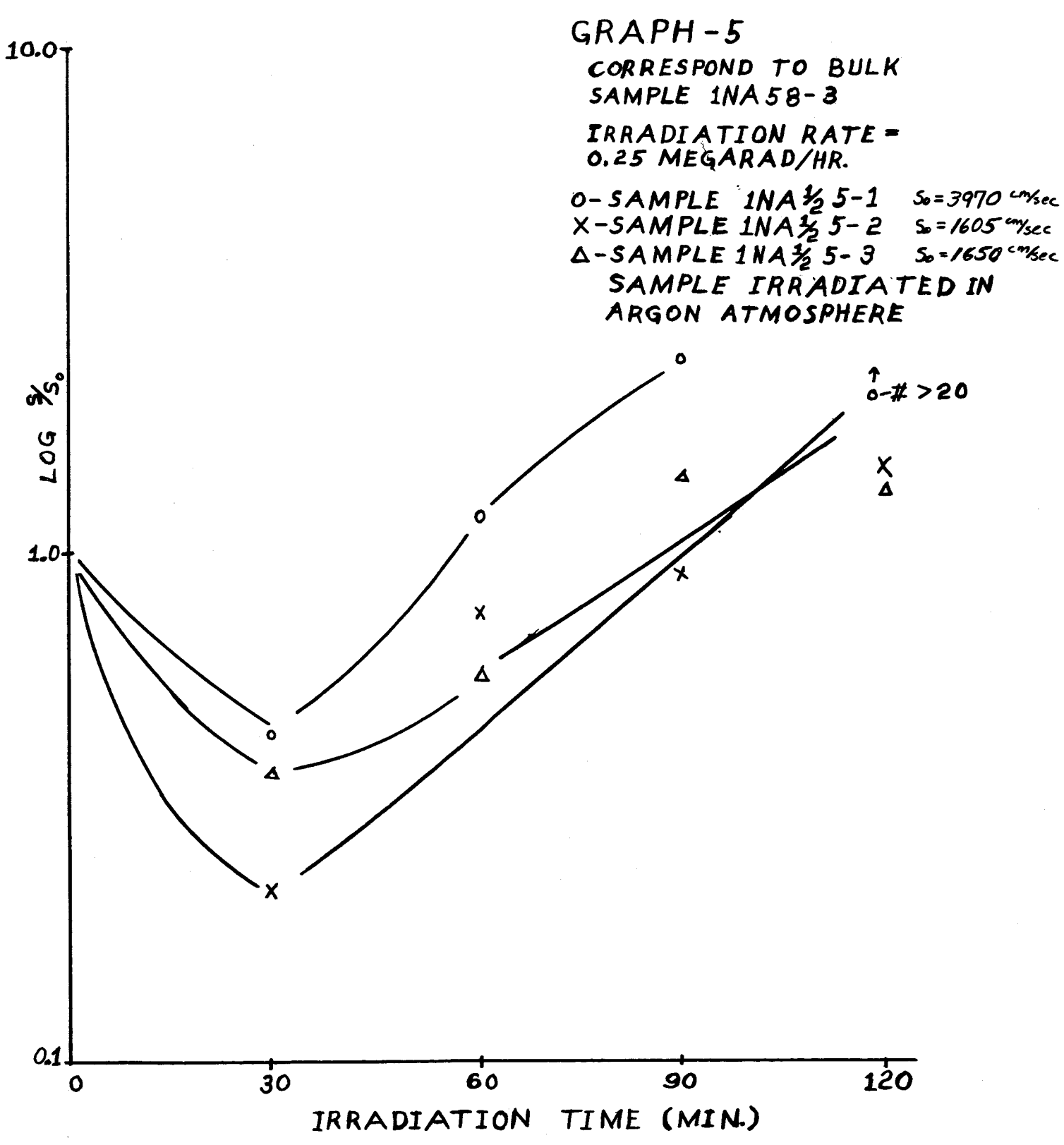
GRAPH-5
CORRESPOND TO BULK SAMPLE 1NA58-3
IRRADIATION RATE = 0.25 MEGARAD/HR.
O-SAMPLE 1NA½ 5-1 S₀=3970 cm/sec
X-SAMPLE 1NA½ 5-2 S₀=1605 cm/sec
Δ-SAMPLE 1NA½ 5-3 S₀=1650 cm/sec
SAMPLE IRRADIATED IN ARGON ATMOSPHERE
O-# >20
LOG S/S₀
10.0
1.0
0.1
0
30
60
90
120
IRRADIATION TIME (MIN.)

GRAPH - 6

CORRESPONDING TO BULK SAMPLE 1NA58-4

IRRADIATION RATE = 0.25 MEGARAD/HR.

O - SAMPLE 1NA ½ 5-4 $S_o = 2620$ cm/sec

X - SAMPLE 1NA ½ 5-5 $S_o = 4720$ cm/sec

Δ - SAMPLE 1NA ½ 5-6 $S_o = 1820$ cm/sec

SAMPLES IRRADIATED IN ARGON ATMOSPHERE

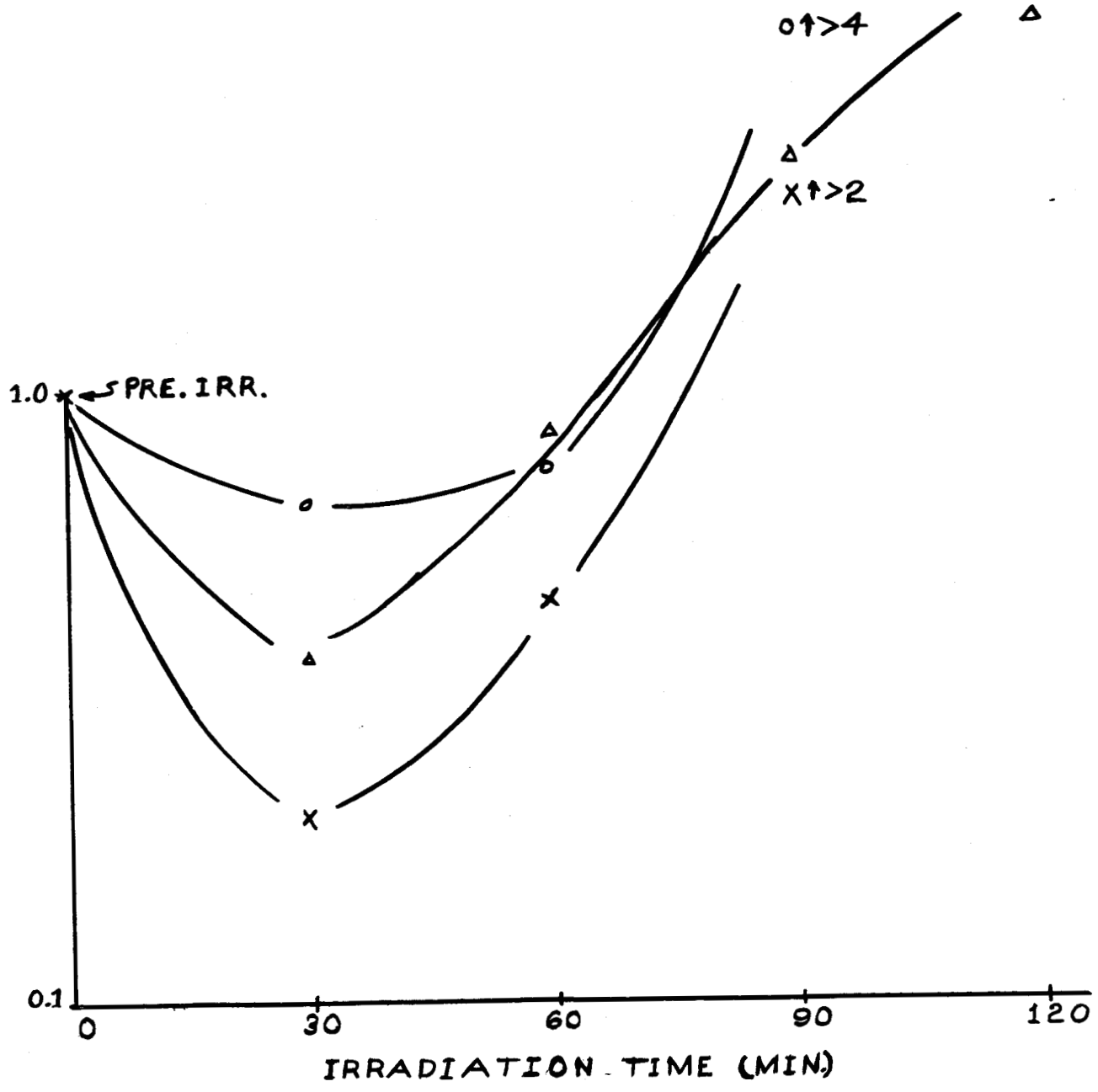

GRAPH - 7

CORRESPOND TO BULK SAMPLE 1NA58-5
IRRADIATION RATE = 0.25 MEGARAD/HR.

O-SAMPLE 1NA½5-7 S_o = 1935 cm/sec
X-SAMPLE 1NA½5-8 S_o = 2620 cm/sec
Δ-SAMPLE 1NA½5-9 S_o = 2790 cm/sec
SAMPLES IRRADIATED IN ARGON ATMOSPHERE

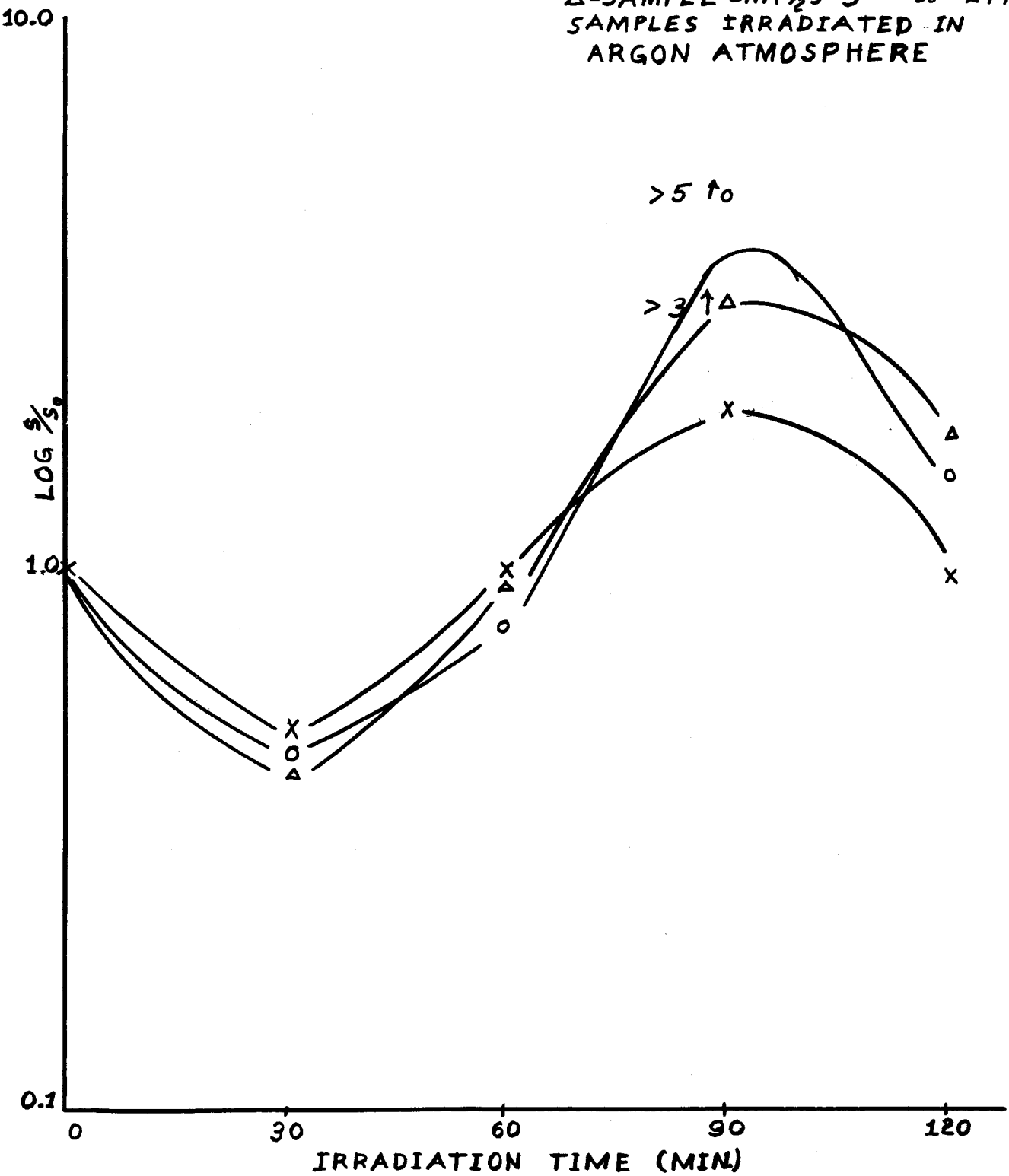

GRAPH-8

O- AVERAGE OF CURVES GRAPH-5
X- AVERAGE OF CURVES GRAPH-6
Δ- AVERAGE OF CURVES GRAPH-7

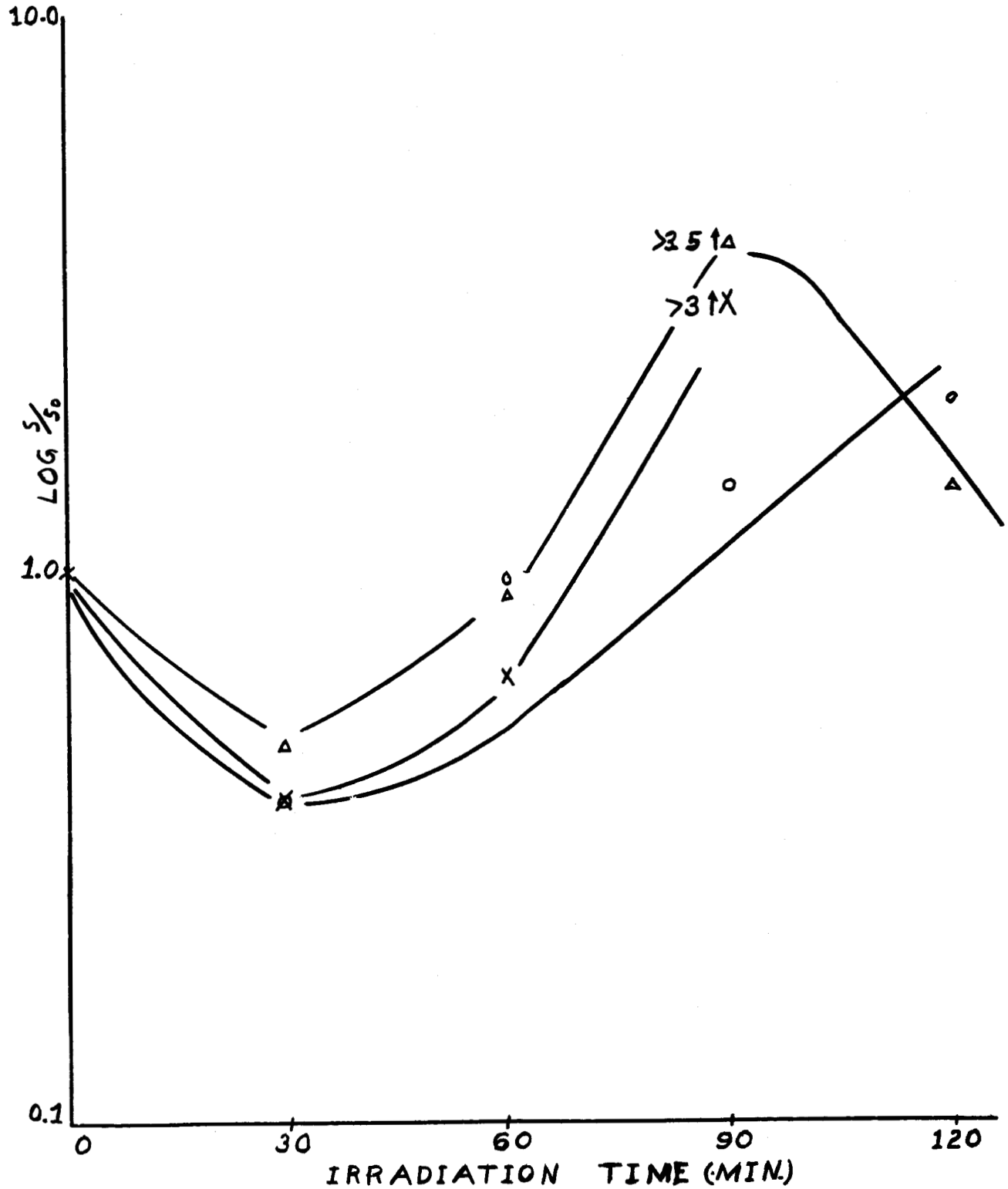

the results for samples 1NA58-3 and 1NA 5-2:

	# 1NA58-3 (τ_b μsec)		# NA½5-2 (S cm/sec)	
	Actual	Corrected	Actual	Corrected
Pre-Irrad.	350	372	1605	1450
1st Irrad.	34.1	33.3	368	338
2nd Irrad.	24.3	24.2	1232	1233
3rd Irrad.	15.9	16.0	1745	1860
4th Irrad.	12.4	12.4	2410	2415

Thus, there is essentially no change in the overall results in assuming D constant. (The total range of D was between 13.1 and 11.6 while 12 was used as its constant value).

Graphs 9, 10, 11, and 12 show graphs of resistivity, Hall coefficient, equilibrium majority carrier concentration, and conductivity mobility as a function of irradiation time. The variations appear to be random; however, the percentage variations are within 10% in all cases, which are on the order of the experimental errors in the measurement procedure.

D. P-Type Silicon

As a continuation of part C, p-type 100 Ω cm silicon was chosen as the next material to study. Again twelve samples, including three bulk samples and nine thin filaments, were constructed, according to the techniques described in part A of this section. The irradiations were carried out in an argon atmosphere, and the results of these irradiations are shown in Graphs 13, 14, 15, 16, and 17.

GRAPH-9

HALL EFFECT MEASUREMENTS
RESISTIVITY
BULK SAMPLES
△ - SAMPLE 1NA58-3
X - SAMPLE 1NA58-4
O - SAMPLE 1NA58-5

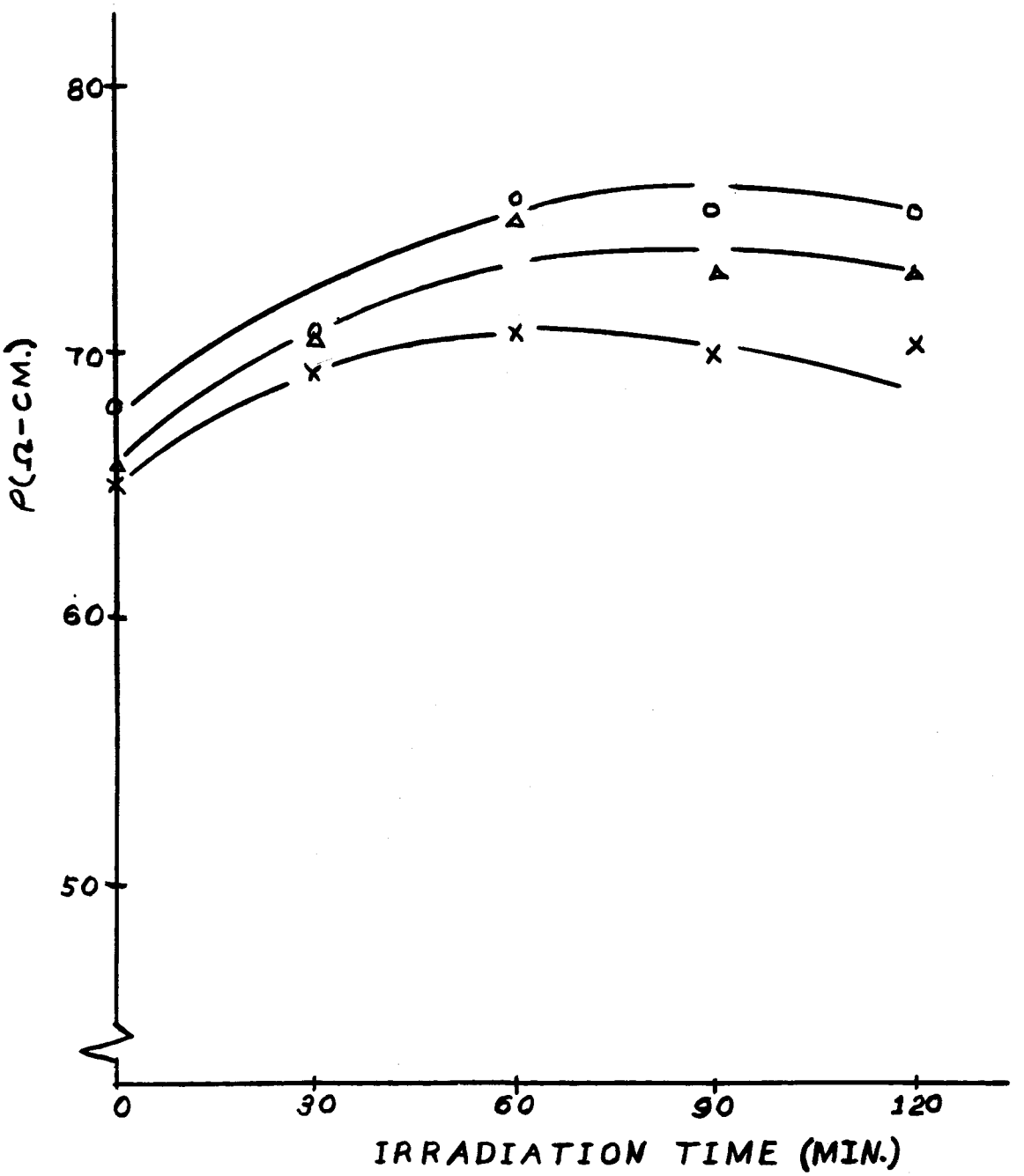

GRAPH-10

HALL EFFECT MEASUREMENTS
HALL COEFFICIENT
BULK SAMPLES
O-SAMPLE-1NA58-3
X-SAMPLE 1NA58-4
Δ-SAMPLE 1NA58-5

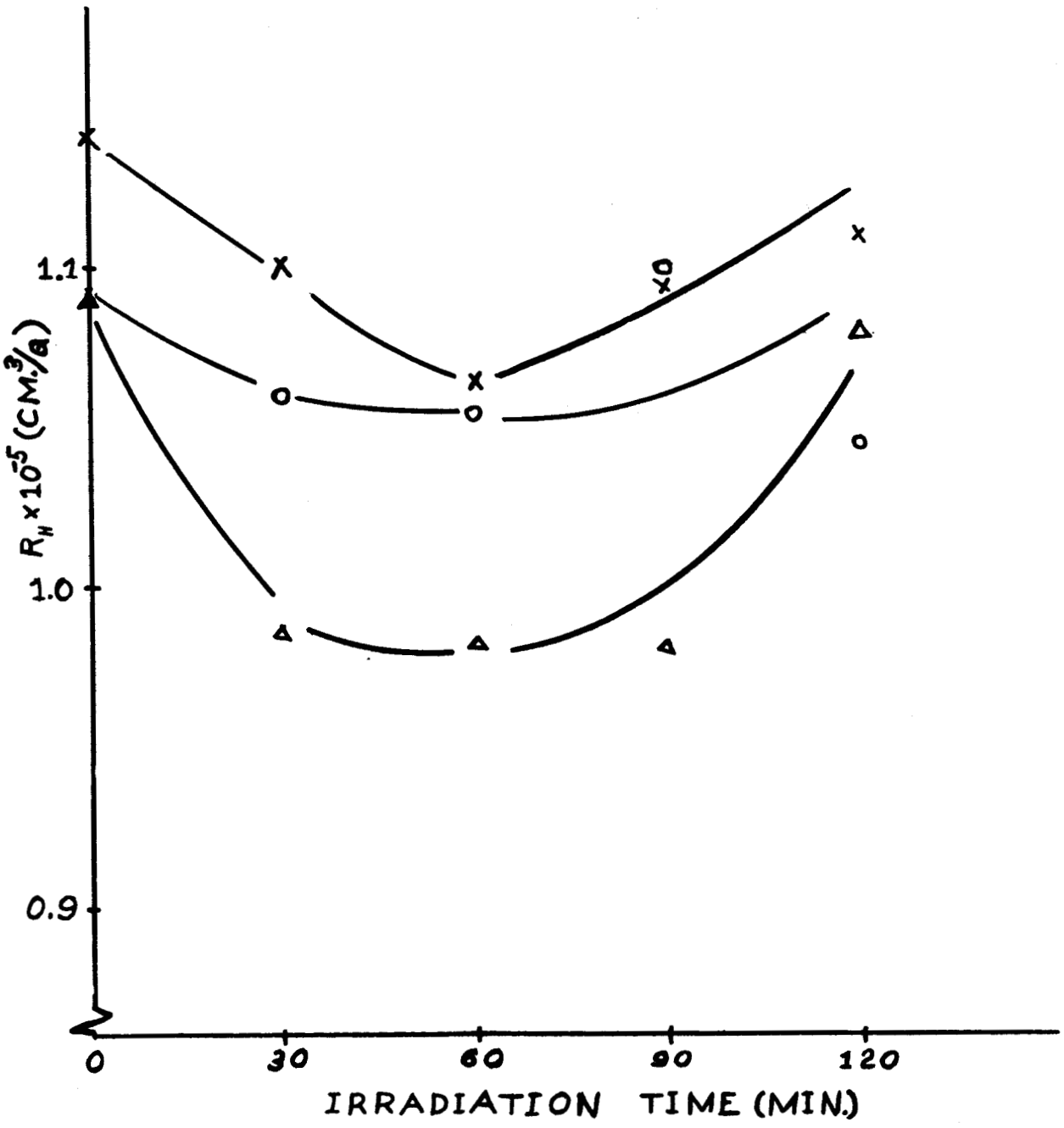

GRAPH-11

HALL-EFFECT MEASUREMENTS
EQUILIBRIUM CONCENTRATION
BULK SAMPLES
O-SAMPLE -1NA58-3
X-SAMPLE 1NA58-4
Δ-SAMPLE 1NA58-5

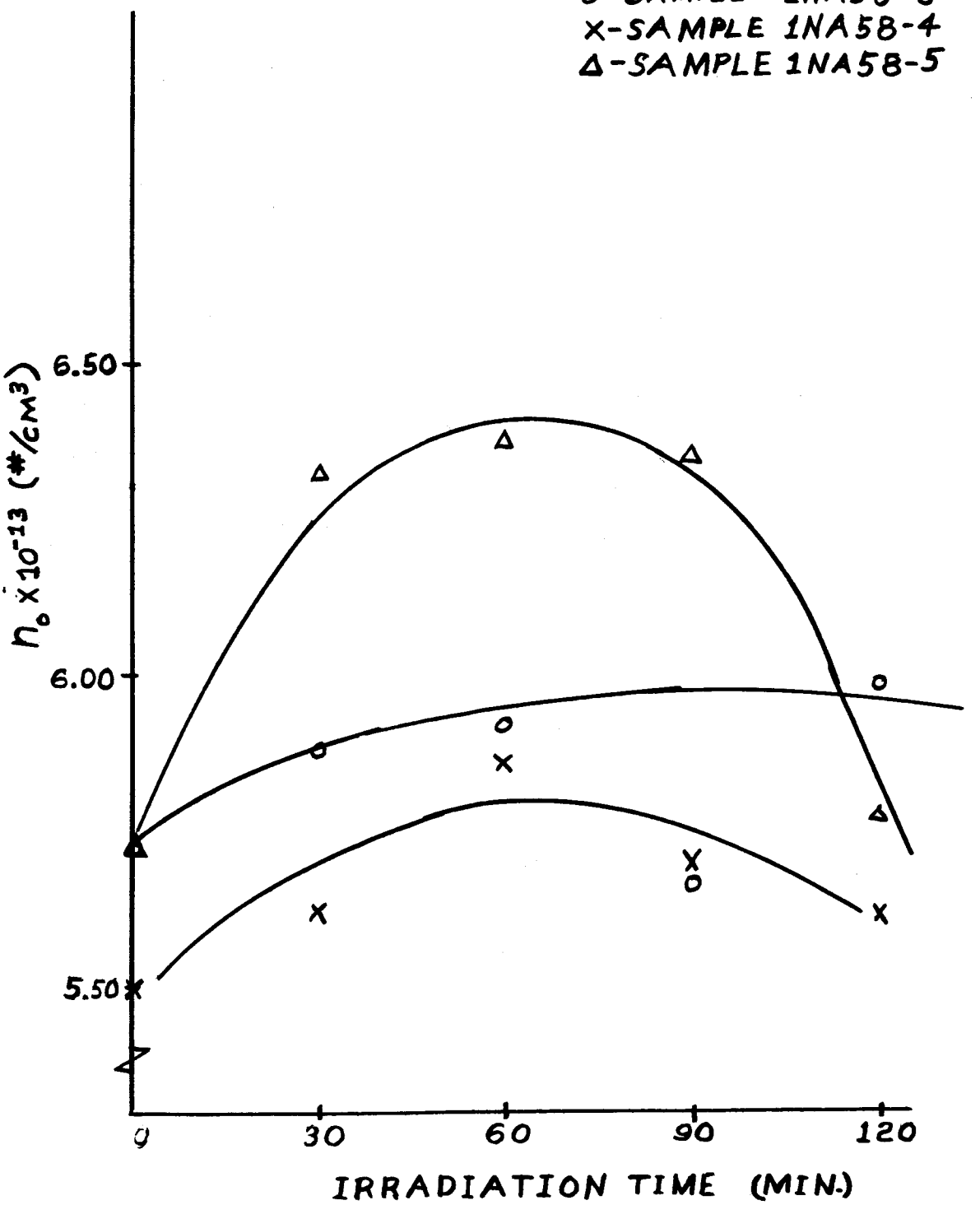

GRAPH-12

HALL EFFECT MEASUREMENTS
CONDUCTIVITY MOBILITY
BULK SAMPLES

O-SAMPLE 1NA58-3
X-SAMPLE 1NA58-4
Δ-SAMPLE 1NA58-5

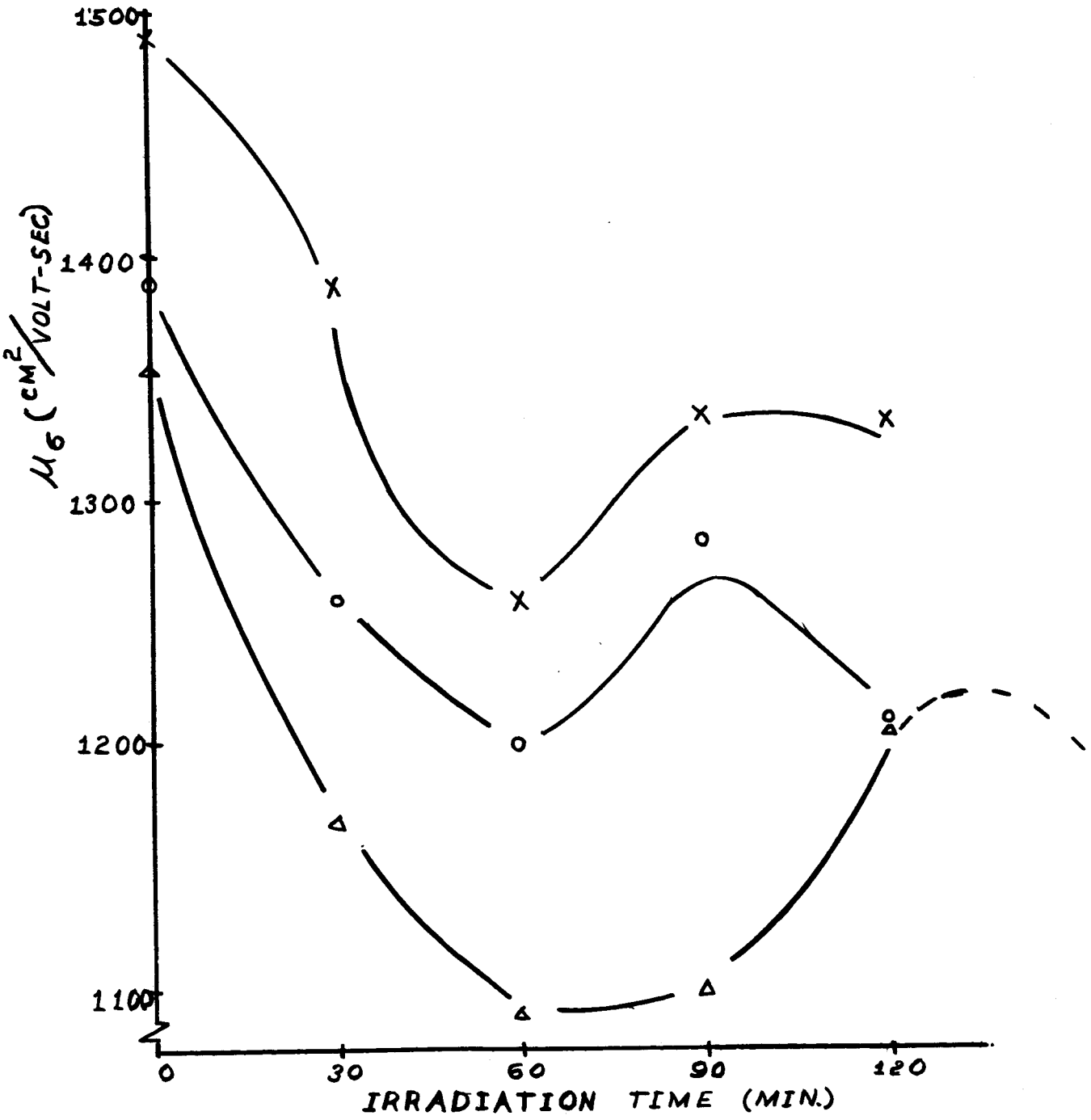

GRAPH-13

O - SAMPLE 1PA58-1 $\tau_{60} = 500\ \mu s$
△ - SAMPLE 1PA58-2 $\tau_{60} = 196\ \mu s$
□ - SAMPLE 1PA58-3 $\tau_{60} = 401\ \mu s$
IRRADIATION RATE = 0.25 MEGARAD/HR

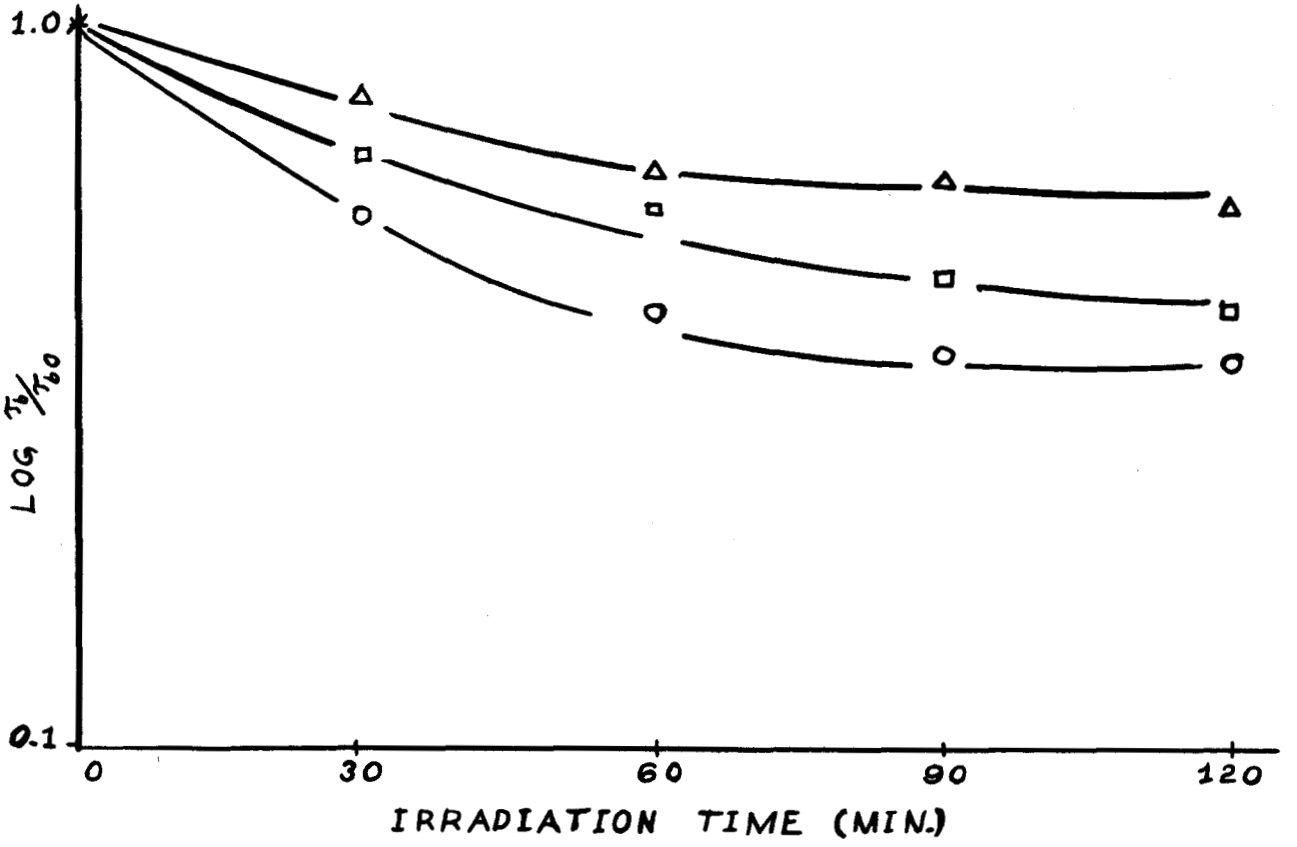

GRAPH-14

O- SAMPLE 1PA $\frac{1}{2}$ 5-1 $S_o = 5140$ CM/SEC
RECTIFYING CONTACTS
Δ- SAMPLE 1PA $\frac{1}{2}$ 5-2 $S_o = 3630$ CM/SEC
RECTIFYING CONTACTS
□- SAMPLE 1PA $\frac{1}{2}$ 5-3 $S_o = 5610$ CM/SEC
IRRADIATION RATE = 0.25 MEGARAD/HR.

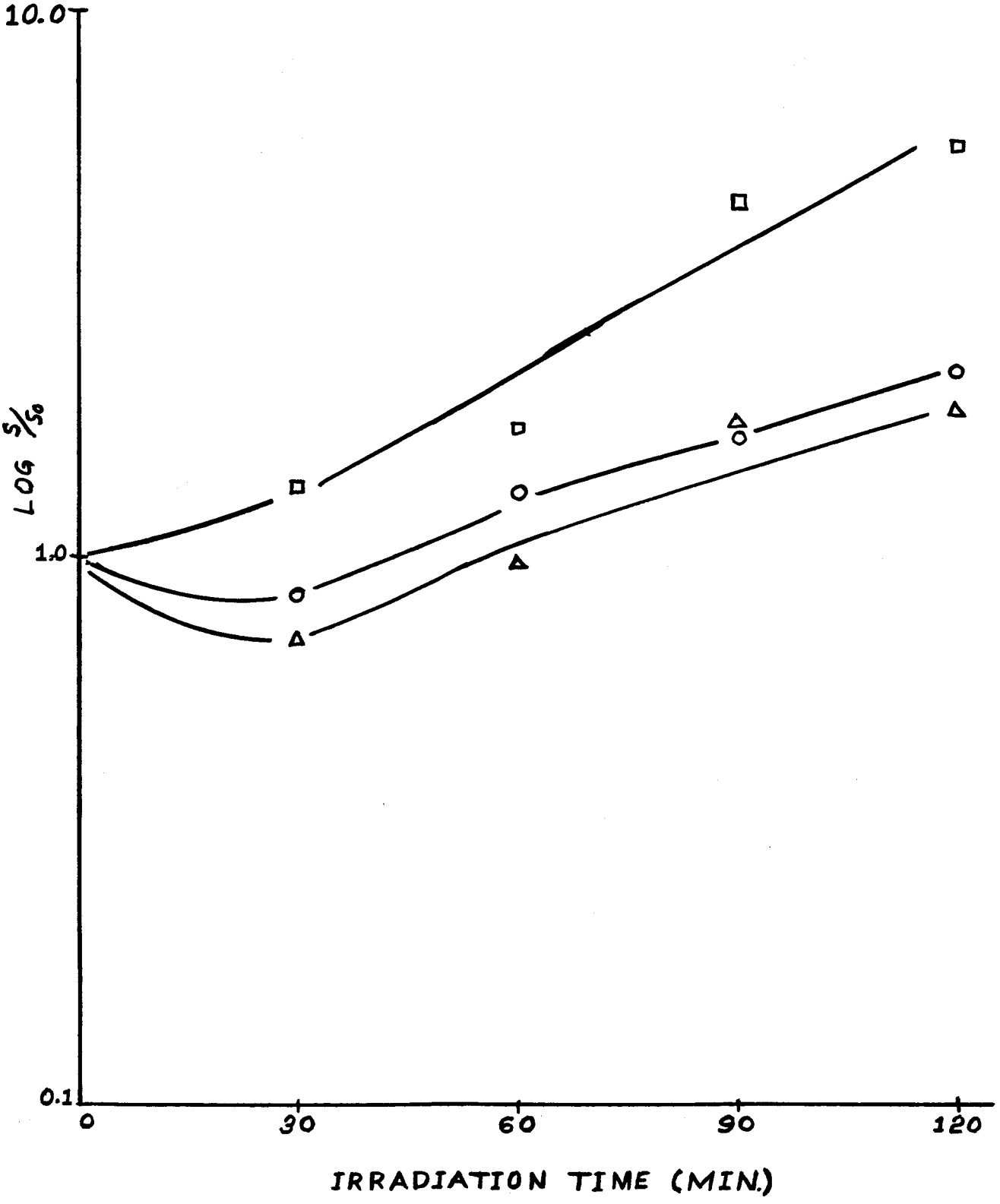

GRAPH -15

O-SAMPLE 1PA½5-4 $S_0 = 4690$ cm/sec
Δ-SAMPLE 1PA½5-5 $S_0 = 5660$ cm/sec
□-SAMPLE 1PA½5-6 $S_0 = 3750$ cm/sec
IRRADIATION RATE = 0.25 MEGARAD/HR.

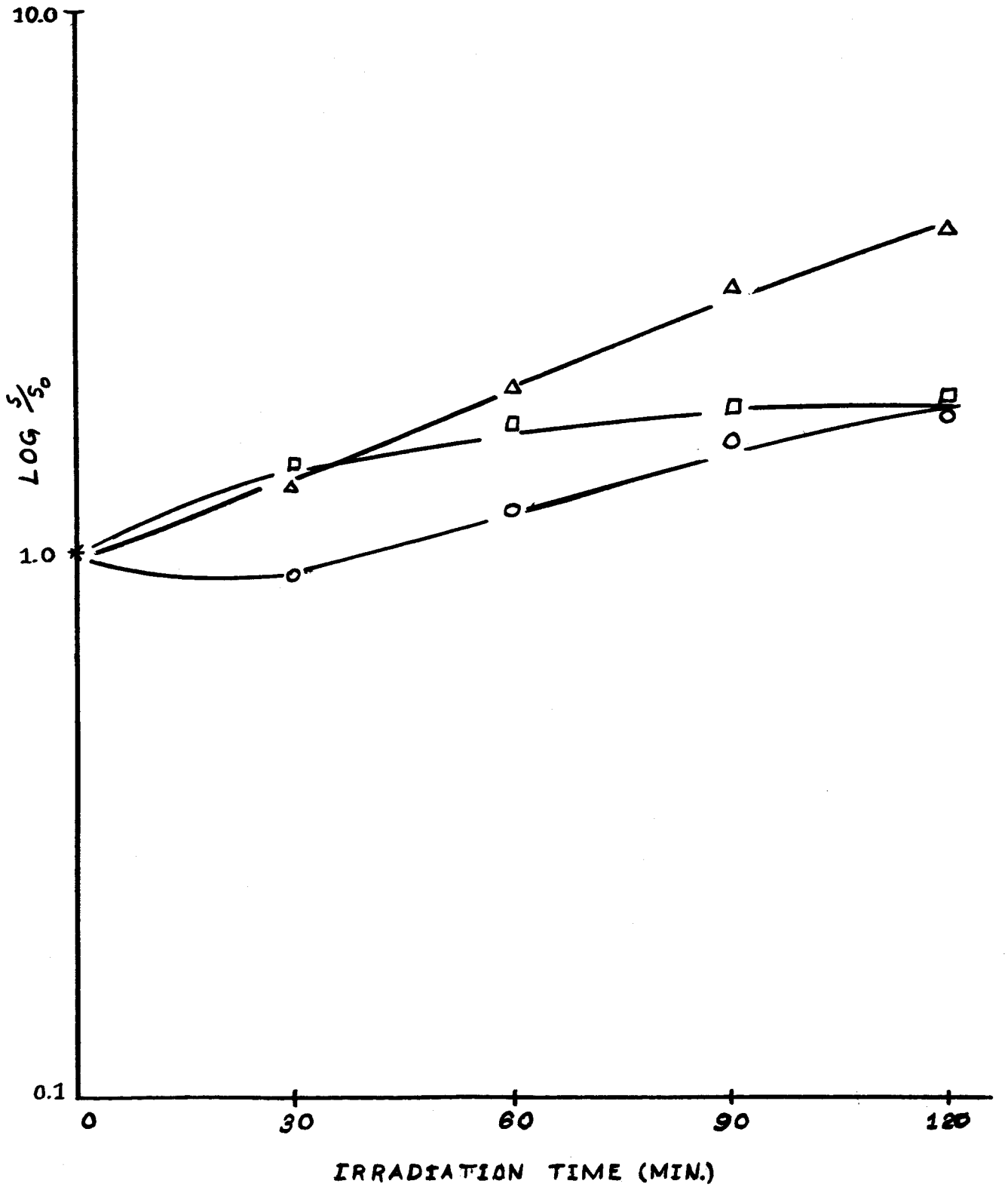

GRAPH -16

O-SAMPLE 1PA ½ 5-7 S_o = 3750 CM/SEC
△-SAMPLE 1PA ½ 5-8 S_o = 4530 CM/SEC
□-SAMPLE 1PA ½ 5-9 S_o = 3960 CM/SEC
IRRADIATION RATE = 0.25 MEGARAD/HR.

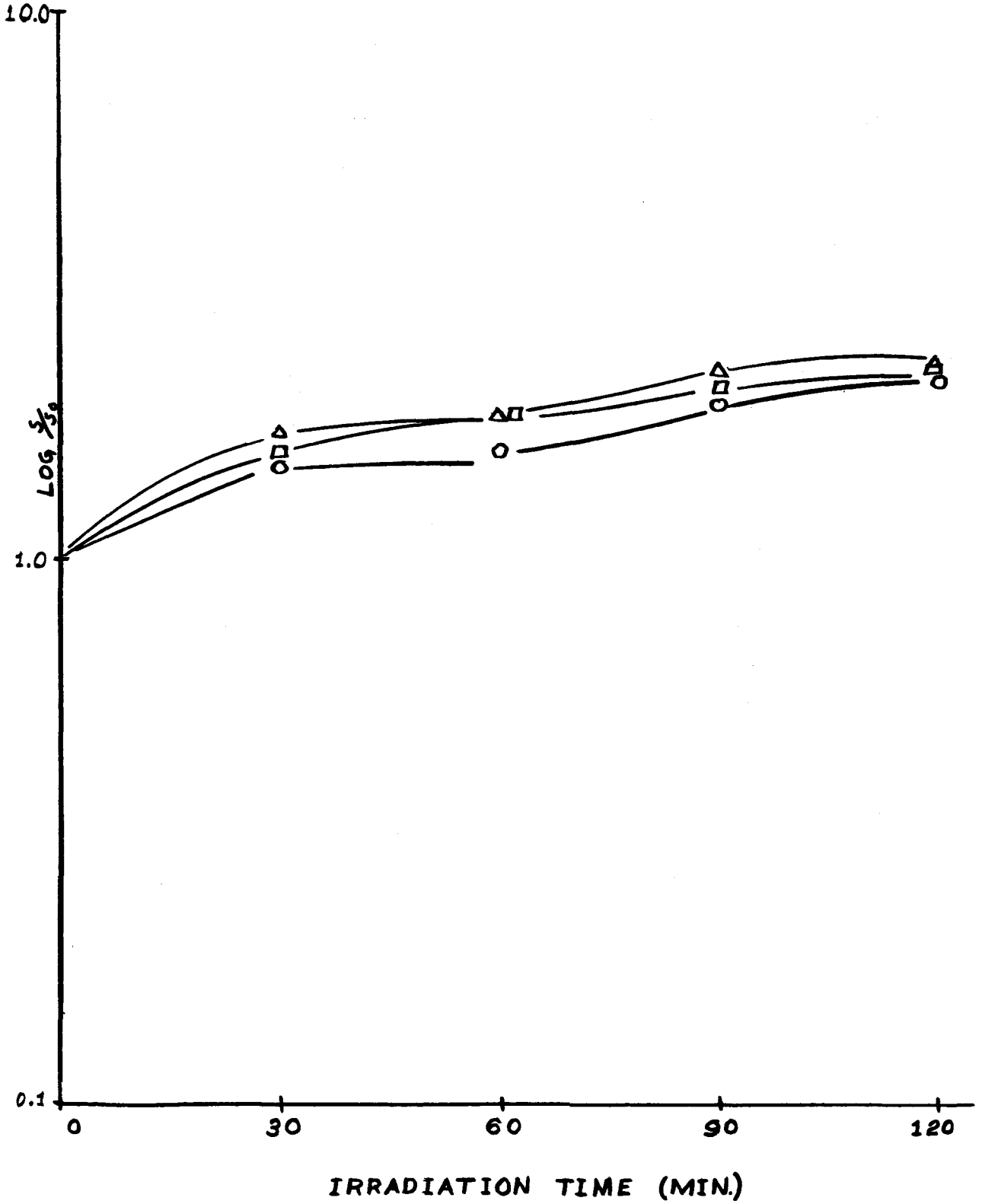

GRAPH-17

O - AVERAGE OF GRAPH-14 $\langle S_o \rangle = 4974$ cm/sec
△ - AVERAGE OF GRAPH-15 $\langle S_o \rangle = 4694$ cm/sec
□ - AVERAGE OF GRAPH-16 $\langle S_o \rangle = 4080$ cm/sec

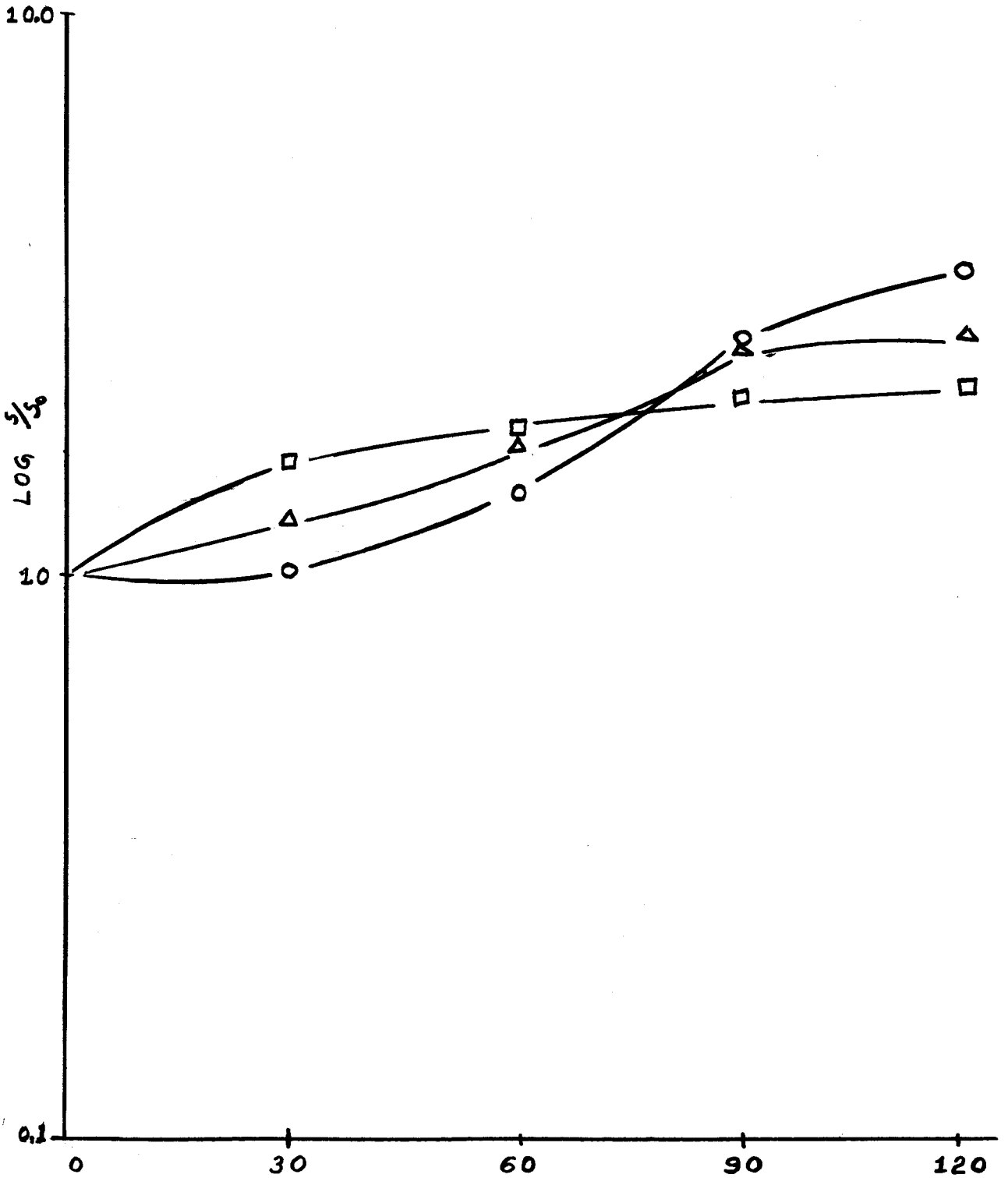

In graph #13, bulk lifetime is plotted as a function of irradiation time in minutes. The initial irradiation causes a decrease for each sample. However, this decrease is on the order of 20 - 45% as compared to two orders of magnitude decrease for the n-type samples. The values of bulk lifetime continue to decrease with each additional irradiation, and seem to approach some asymptotic value. The marked contrast between the effects of gamma irradiation on bulk lifetime in n and p type silicon should be noted in graphs # 1, 4, and 13.

Graphs 13, 14, and 15 each show the variations of surface recombination velocity for a set of three thin filaments with the same bulk lifetime as a function of irradiation time in minutes. In graph # 13, samples 1PA½5-1 and 2 exhibit a relative "minimum" in S while sample 1PA½5-3 shows a monotonically increasing value of S as a function of irradiation time. An examination of the v-i characteristics of these three samples showed that 1PA½5-1 and 1PA½5-2 had injecting or "rectifying" contacts (characterized by a non-linear v-i characteristic) while 1PA½5-3 had a linear v-i characteristic, indicating non-injecting contacts. The apparent minima appear to be traceable to the introduction of appreciable numbers of minority carriers by the injecting contacts.

In graph #14, sample 1PA½5-4 also had injecting contacts, and again exhibited a relative minimum in S. Samples 1PA½5-5 and 6 both showed values of S that continuously increased increased with irradiation time.

In graph #16, samples 1PA½5-7, 8, and 9 all exhibited a continuously increasing value of S, and all had ohmic contacts.

A survey of the data for p-type silicon showed that all samples with ohmic contacts had values of S that increased continuously with irradiation, while only those samples with injecting contacts exhibited a relative minimum in S.

The electroless nickel plating solution used is known to contain a large percentage of phosphorous. This phosphorous can, and often does, create a junction effect when extreme precaution is not taken in the process of plating the contacts. This problem is not present when plating n-type material. This aspect of the effect of irradiation on surface recombination is an interesting problem in itself, and will be investigated.

E. Summary

In summary, the bulk lifetime in silicon decreases with increasing gamma radiation; n-type material exhibiting a much more drastic change than p-type material.

Surface recombination velocity has a relative minimum value for n-type silicon and for p-type silicon with injecting contacts. For p-type silicon the value of S monotonically increases with increasing gamma radiation.

Hall data taken on all samples indicates that no definite trends in mobility or carrier concentrations are to be expected over the gamma doses considered in this study.

A mathematical model to describe the effects of free surface damage reported is presently being considered and will be described in a future report.

II. Surface Potential-Field Effect Studies

A. Introduction

An oxide coating on a silicon surface will passivate that surface to a great extent. The oxide can be thermally grown in either a pure oxidizing atmosphere or one which has had impurities introduced. In either case certain states or bound charge centers will be present in the oxide. The density and distribution of these charge centers throughout the oxide, along with the density of bound charge centers at the oxide-silicon interface, influences the surface conductance of silicon to a great extent. The surface conduction (also called the change in conduction with respect to that of the charge neutral bulk of the material) is due to a change in electron and/or hole concentration at and near the surface region with respect to the bulk concentration. This change in surface conductance (in many cases) seriously effects the external volt-ampere characteristics of a device and, in some devices such as the MOS Transistor, is the main mechanism of operation.

For this reason the determination of the above mentioned density and distribution of bound charge centers in the oxide is of great importance both in device construction technology and the theoretical prediction of device characteristics. The field effect technique[2] is helpful in yielding information on both distribution and density of these oxide states. This technique involves the measurement of the conductance of a surface channel of a particular material as a function of an applied normal electric field. Both the magnitude and direction of this $\bar{E}$ field

determine whether electrons or holes or either is the majority current carrying specie in the surface channel. A typical sample along with the requisite circuitry to observe the field effect is shown in Figure 1.

The surface conductivity can be theoretically predicted for a specific material for which certain parameters are known (see Appendix A). The theoretical and experimental ΔG vs V_g curves must be shifted vertically so that both minima occur at the same value of ΔG[3]. Example curves are given in Figure 2.

The theoretical curve is plotted with surface potential (difference between the electrostatic potential at the surface and in the bulk where charge neutrality prevails) noted on the curve. Since the surface conductivity is a function only of surface potential, horizontal lines drawn on the curves corresponding to certain values of surface potential for the theoretical case will also denote those same surface potentials for the experimental curve.[3] The difference in charge (Q_s) between the theoretical and experimental curves for a given surface potential is the value of bound charge centers in the oxides which have charge transfer times so great that the polarity of these centers does not change over a period of the gate to substrate voltage. Hence, by varying the gate to substrate frequency one can obtain different curves of ΔG vs V_g . By deducing a charge transfer time for each frequency used, one can categorize the bound charge centers as to charge transfer time or physical distance from the oxide-silicon interface to the charge centers.

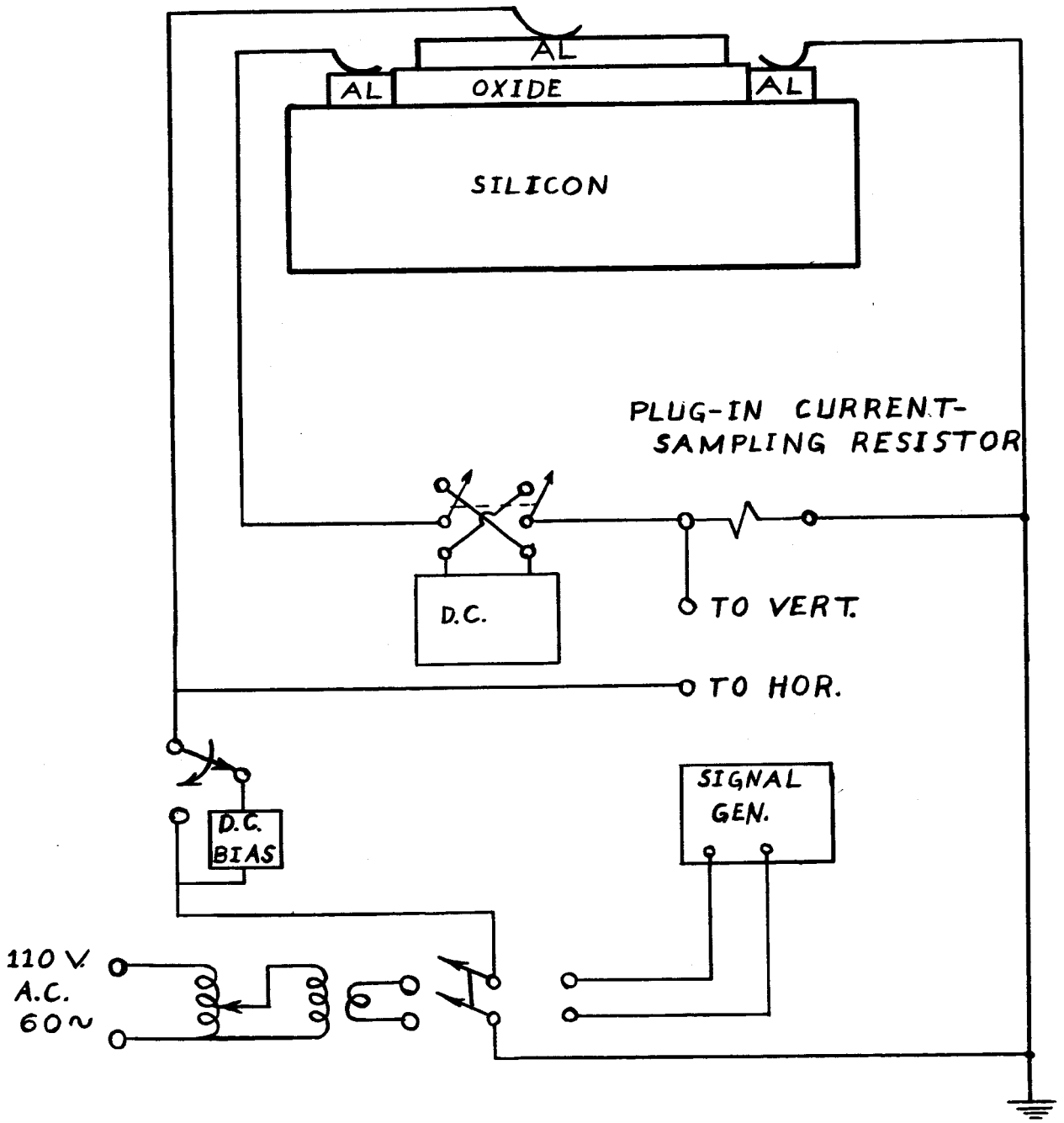

Figure 1. Field-Effect Circuitry

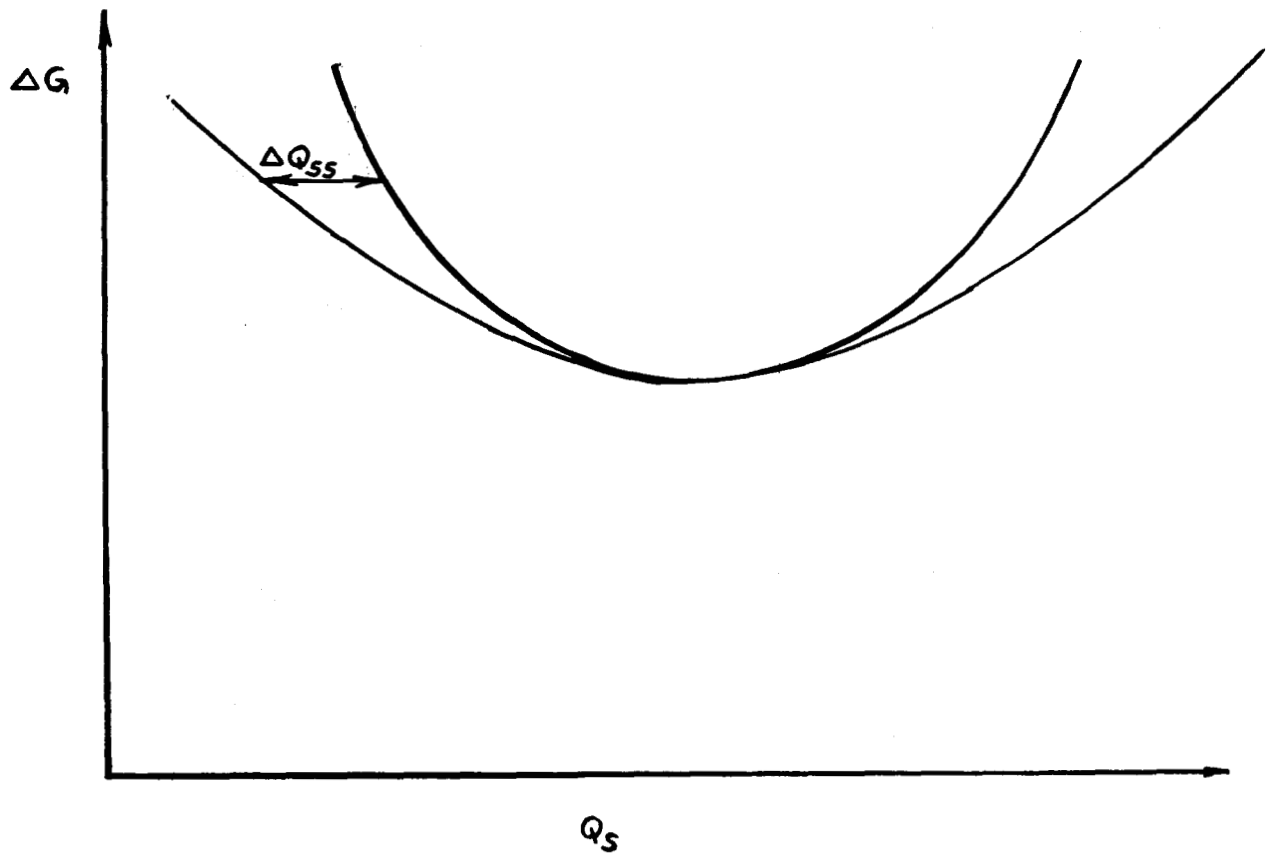

Figure 2. Typical Experimental and Theoretical Relationships between Surface Conductivity and Total Surface Charge

A major effort by one group at this laboratory is directed toward producing devices which can be used in these field effect measurements. After making such devices, comparison of graphs of the surface conductivity vs Q_s obtained before and after irradiation will make it possible to deduce density and distribution changes of the bound charge centers in the oxide. The following sections will outline design and construction techniques for preparing the field effect devices.

B. Surface Polishing and Cleaning

The silicon samples to be used in the fabrication of field effect devices were sliced from a silicon ingot on a wafering machine. The samples of the first group lapped with #100 grit, #800 grit, 10μ grit, 1μ grit, 0.3μ grit, and .05μ grit. The surfaces on these samples were covered with very small hole-type irregularities. It is believed that if the surfaces are lapped with grit sizes #100, #200, #400, #800, 50μ and 10μ in that order and then polished with 1μ, 0.3μ and .05μ polishing powders in that order that the surface irregularity problem will be eliminated.

It may be well to mention at this point that there is only one surface polishing procedure which will hopefully yield reproducable surfaces. That procedure is simply to lap or polish long enough with each material so that the deepest surface dislocations present are due not to the previous step of the process but to the one presently used.

After a well-polished surface is present on the samples, they are cleaned by submerging them in trichloroethylene and

ultrasonically cleaning them. After this step the following surface cleaning procedure is used:

(a) Boil in trichloroethylene for 30 sec. decanting and boiling again for 30 sec.

(b) Immerse in room temperature methyl alcohol for 30 sec.

(c) Flush 5 times in room temperature demineralized distilled water.

(d) Immerse for 30 min. in 80°C H_2SO_4.

(e) Flush 5 times in room temperature demineralized distilled water.

(f) Immerse for 30 min. in 80°C HNO_3.

(g) Flush 10 times in room temperature distilled demineralized water.

(h) Store in methyl alcohol until loading into furnace (usually only about 2 or 3 min.).

The furnace is kept at 1250°C during the oxide growth. Oxygen is bubbled through 75°C water at a rate of 2 $\ell/_{min}$ and passed through the 40 mm I.D. quartz furnace tube. Naturally all quartz tubing and associated oxidation system equipment is cleaned before the oxidation of the silicon. The samples of Si are oxidized for 60 min. yielding an oxide thickness on the order of 5000 Å.

C. Oxide Parameters

The meaningful figure of merit of an oxide is the D.C. resistance between the substrate and the aluminum gate evaporated on the oxide surface. For these measurements an array of 30 mil Al dots was evaporated onto the oxide and 2 small sections of the

oxide were ground away. One section was used to make electrical contact to the substrate. The other was used to check this contact. A 5 mil Ni wire was positioned vertically by means of a micro-manipulator on each Al dot. The resistance from dot to substrate was found to be on the order of 10^{13} ohms and that from the substrate to the second ground away portion was 10^{8} ohms which is quite reasonable considering the rough surface and the Ni loop contact.

The capacitance between each dot and the substrate was measured at 1000 cycles/sec. and ranged from 23 to 28 $\mu\mu f$. From this and the oxide thickness it was deduced that the relative permittivity (dielectric constant) of the oxide was approximately 4.

The oxide thickness was measured by the evaporation of Al over a portion of another sample of the same oxidation group. A portion of the oxide had been etched away on this sample and the Al evaporation was one large area, a portion of which was on the oxidized Si. The completely reflecting discontinuity caused by this evaporation was observed on a Leitz interference microscope. The oxide was approximately 5000 Å thick by this measurement technique.

D. Device Design

The surface geometry and a cross-section of a device to be made is shown in Figure 3.

The source and drain holes will be cut into the oxides by means of Kodak Photo Resist techniques as follows:

(a) Fresh oxide is coated with KPR.

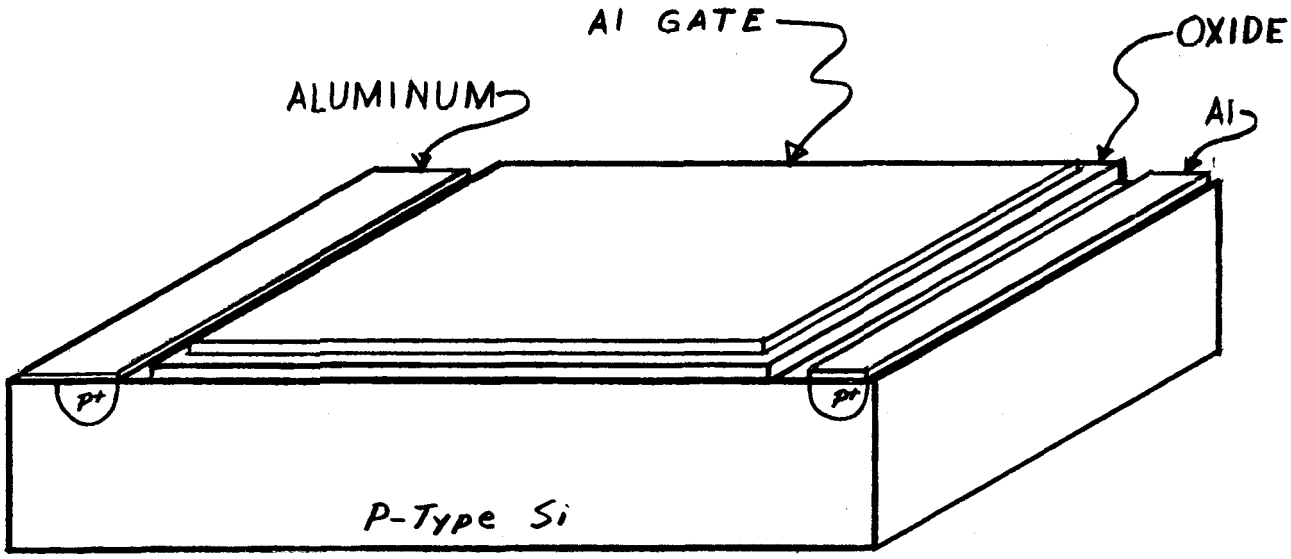

Figure 3. Field Effect Measurement Device

(b) While still wet and until dry the sample is whirled about an axis normal to and through the center of its circular cross section surfaces at approximately 1750 rpm.

(c) The coating of KPR is baked on for 1 hr. at 90°C.

(d) Oxide and mask are positioned in a camera and exposed.

(e) KPR coating is developed.

(f) An etch consisting of

40 gm NH_4F

60 ml H_2O

9 ml HF

which has an etch rate of approximately 800Å/min. is used to remove unwanted oxide.

(g) Exposed KPR is stripped off in 80°C H_2SO_4.
The sample is then cleaned and a 1 mil brass evaporation mask is positioned with respect to the sample. The sample and mask assembly are then placed in a vacuum system and source, drain and gate are simultaneously evaporated onto the sample at a vacuum of about 8×10^{-5} mm of Hg.

III. Solar Cell - Solutions for the Short Circuit Current

This section describes a theoretical investigation of the effects of surface recombination velocity and diffusion length on the short circuit current of a solar cell. This study shows that for low absorption coefficients the short circuit current is independent of the surface recombination velocity and a strong function of the diffusion length. For high absorption coefficients the opposite is true.

List of symbols:

α = absorption coefficient, cm^{-1}

$\bar{n}$, $\bar{p}$ = excess minority carrier density in p and n region respectively, cm^{-3}

τ_n, τ_p = minority carrier lifetime S, sec.

D_n, D_p = diffision coefficient for electrons and holes respectively, cm^2 sec^{-1}

S_1, S_2 = surface recombination velocity of front side of cell and back side of cell respectively, cm sec^{-1}

D_n, D_p = diffusion length for electron and holes, cm

$g(x)$ = the rate of electron-hole pairs generated at any depth, cm^{-3} sec^{-1}

I = monochromatic photon flux entering cell, cm^{-2} sec^{-1}

μ_n, μ_p = electron and hole nobilities respectively, $cm^2 volt^{-1} sec^{-1}$

$\bar{\mathcal{E}}(x)$ = electric field strength, volt cm^{-1}

q = electronic charge, 1.6×10^{-19} coul

k = Boltzmann constant, eV $-{}^{o}K^{-1}$

T = absolute temperature ^{o}K

R_n, R_p = net generation-recombination rate for electron and holes respectively, cm^{-3} sec^{-1}

J_n = electron current density, amp cm^{-2}

J_p = hole current density, amp cm^{-2}

J_T = Jn + Jp, amp cm^{-2}

X = distance from light exposed surface of cell, cm

W = distance from light exposed surface of cell to front side of p-n junction, cm

A = distance from light exposed surface of cell to back side of p-n junction, cm

B = distance from light exposed surface of cell to back surface of cell, cm

$\bar{J}$ = normalized current

A. Introduction

The model shown in Figure 4 will be used.

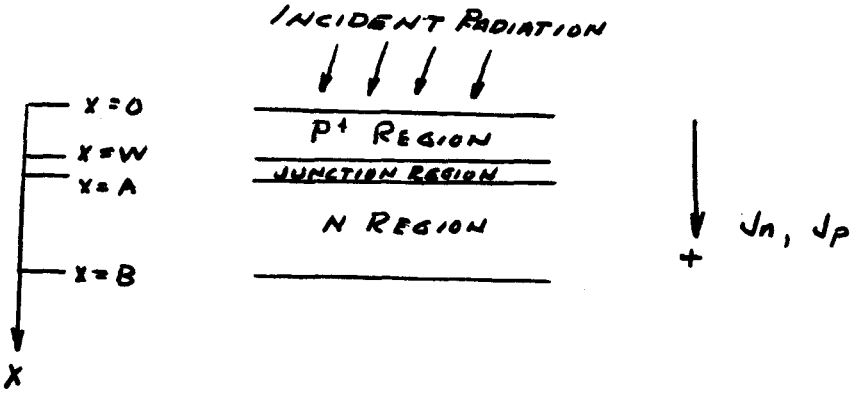

Figure 4. Sketch of Photo Cell Considered with Different Regions Denoted

The following simplifying assumptions were made in order to solve the problem:

(1) Current carried by diffusion only

(2) Steady state conditions prevail

(3) Boltzmann boundary conditions are valid

(4) No recombination in the depletion region

(5) $g(x) = \alpha I \exp(-\alpha x)$

(6) $W L_n^{-1} << 1$

(7) $(B-A) L_p^{-1} >> 1$

(8) $R_n = -\bar{n}\,\tau_n^{-1}$; $R_p = -\bar{p}\,\tau_p^{-1}$; $\tau_n = \tau_p$

With these assumptions two different cases need to be considered. First the case when $\alpha W << 1$ which leads to the following expression for the short circuit current

$$J_{s.c.} = -qI\alpha \left[W + \frac{L_p}{1 + \alpha L_p} \right] \qquad (1)$$

The case for $\alpha W >> 1$ yields the following expression for short circuit current

$$J_{s.c.} = -q\frac{I}{\alpha} \left[\frac{\alpha + S_1 D_n^{-1}}{1 + S_1 D_n^{-1} W} \right] \qquad (2)$$

B. General Solution for the Current of A Solar Cell

The ambipolar continuity equation is

$$\frac{\partial \bar{n}}{\partial t} = g(x) - R_n + \mu_n \cdot \bar{E}(x) \frac{\partial \bar{n}}{\partial x} + D_n \frac{\partial^2 \bar{n}}{\partial x^2}$$

Under the previously mentioned assumptions, this reduces to the following in the P^+ region

$$\frac{d^2\bar{n}}{dx^2} - \frac{\bar{n}}{L_n^2} = \frac{\alpha I}{D_n} \exp(-\alpha x)$$

The boundary conditions are

at x = o $\quad J_n(0) = q S_1 \bar{n} = q D_n \left.\frac{d\bar{n}}{dx}\right|_{x=0}$

at x = w $\quad \bar{n}(W) = N_{po}\left[\exp\left(\frac{qV}{kT}\right) - 1\right]$

$$\bar{n}(x) = \beta_1 \sinh\frac{x}{L_n} + \beta_2 \cosh\frac{x}{L_n} - \frac{\alpha I \tau_n}{\alpha^2 L_n^2 - 1}\exp(-\alpha x)$$

Using the preceding boundary condition yields:

$$\beta_1 = \frac{L_n S_1' N_{po}(e^{qV/kT} - 1) + L_n S_1' C_n e^{-\alpha W} - (S_1' + \alpha) L_n C_n \cosh\left(\frac{W}{L_n}\right)}{L_n S_1' \sinh\left(\frac{W}{L_n}\right) + \cosh\left(\frac{W}{L_n}\right)}$$

$$\beta_2 = \frac{N_{po}(e^{qV/kT} - 1) + C_n e^{-\alpha W} + [S_1' + \alpha] L_n C_n \sinh\left(\frac{W}{L_n}\right)}{L_n S_1' \sinh\left(\frac{W}{L_n}\right) + \cosh\left(\frac{W}{L_n}\right)}$$

where $\quad S_1' = \frac{S_1}{D_n} \; ; \quad C_n = \frac{\alpha I \tau_n}{\alpha^2 L_n^2 - 1}$

assume that $\quad \frac{W}{L_n} \ll 1$

$$\beta_1 \cong \frac{L_n S_1' [N_{po}(e^{qV/kT} - 1) + C_n e^{-\alpha W}] - (S_1' + \alpha) L_n C_n}{1 + S_1' W}$$

$$\beta_2 \cong \frac{N_{po}(e^{qV/kT} - 1) + C_n e^{-\alpha W} + (S_1' + \alpha) C_n W}{1 + S_1' W}$$

Likewise in the N-Region

$$\frac{d^2}{dx^2}\bar{p} - \frac{\bar{p}}{L_p^2} = -\frac{\alpha I}{D_p}\exp(-\alpha x)$$

$$\bar{p}(x) = \beta_3 \sinh\frac{x-A}{L_p} + \beta_4 \cosh\frac{x-A}{L_p} - C_p e^{-\alpha x}$$

where

$$L_p^2 = \tau_p D_p \; ; \quad C_p = \frac{\alpha I \tau_p}{\alpha^2 L_p^2 - 1}$$

The boundary conditions are:

at x = A; $\quad \bar{p}(A) = P_{no}\left[\exp\left(\frac{qV}{kT}\right) - 1\right]$

at x = B; $\quad J_p(B) = q \bar{p} S_2 = -q D_p \left.\frac{d}{dx}\bar{p}\right|_{x=B}$

$$\beta_3 = \frac{(S_2' - \alpha) C_p e^{-\alpha B} - [P_{no}(e^{qV/kT} - 1) + C_p e^{-\alpha A}]\left[L_p^{-1}\sinh\left(\frac{B-A}{L_p}\right) + S_2' \cosh\left(\frac{B-A}{L_p}\right)\right]}{L_p^{-1}\cosh\left(\frac{B-A}{L_p}\right) + S_2' \sinh\left(\frac{B-A}{L_p}\right)}$$

$$\beta_4 = P_{no}\left(e^{qV/kT}-1\right) + C_p e^{-\alpha A}$$

where $$S_2' = \frac{S_2}{D_p}$$

assume that $$\frac{B-A}{L_p} >> 1$$

$$\beta_3 \cong -P_{no}\left(e^{qV/kT}-1\right) - C_p e^{-\alpha A}$$

$$J_n(W) = q D_n \left.\frac{d\bar{n}}{dx}\right|_{x=W}$$

$$J_n(W) = q D_n \left[\frac{\beta_1}{L_n}\cosh\left(\frac{W}{L_n}\right) + \frac{\beta_2}{L_n}\sinh\left(\frac{W}{L_n}\right) + C_n\alpha e^{-\alpha W}\right]$$

$$J_p(A) = -q D_p \left.\frac{d}{dx}\bar{p}\right|_{x=A}$$

$$J_p(A) = -q D_p\left[\frac{\beta_3}{L_p} + C_p\alpha e^{-\alpha A}\right]$$

assume $$J_p(A) = J_p(W)$$

$$J_T = J_n(W) + J_p(W)$$

$$J_T = \left\{q\frac{D_n}{L_n}\left[\frac{L_n S_1' + W}{1+S_1'W}\right]N_{po} + q\frac{D_p}{L_p}P_{no}\right\}\left(e^{qV/kT}-1\right)$$

$$+ q\frac{D_n}{L_n^2}C_N\left\{\frac{\left[L_n^2 S_1' + W + \alpha L_n^2(1+S_1'W)\right]e^{-\alpha W} - (S_1'+\alpha)(L_n^2-W^2)}{1+S_1'W}\right\}$$

$$- q\frac{D_p}{L_p^2}C_p\left\{\alpha L_p^2 - L_p\right\}e^{-\alpha W}$$

Setting V = 0 yields the short circuit current

$$J_{T\,s.c.} = q\frac{D_n}{L_n^2}C_n\left\{\frac{\left[L_n^2 S_1' + W + \alpha L_n^2(1+S_1'W)\right]e^{-\alpha W} - (S_1'+\alpha)(L_n^2-W^2)}{1+S_1'W}\right\}$$

$$- q\frac{D_p}{L_p^2}C_p\left\{\alpha^2 L_p^2 - L_p\right\}e^{-\alpha W}$$

Let

$$b = \frac{\mu_n}{\mu_p} \quad ; \quad \gamma = \frac{C_n}{C_p} = \frac{\alpha^2 L_p^2 - 1}{b\alpha^2 L_p^2 - 1}$$

define $$\bar{J} = J_{r.s.c.} \left[q \frac{D_p C_p}{W} \right]^{-1}$$

$q \frac{D_p C_p}{W}$ represents a current that would result from a constant hole-electron generation throughout the P^+ region.

$$\bar{J} = \frac{\gamma b \left[S_1' W (e^{-\alpha W} - 1) - \alpha W \right]}{1 + S_1' W} + \left[(\gamma b - 1)\alpha W - \frac{W}{L_p} \right] e^{-\alpha W}$$

$\bar{J}$ versus $\frac{W}{L_p}$ is plotted holding αW constant in Figure 5. This shows that for $\alpha W > 10^{-1}$, $\bar{J}$ is approximately independent of $\frac{W}{L_p}$. In Figure 6 $\bar{J}$ is plotted against $S_1' W$ holding αW constant. This shows that for $S_1' W < 10^{-1}$ $\bar{J}$ is independent of $S_1' W$ while for $\alpha W \leq 10^{-1}$, $\bar{J}$ is independent of $S_1' W$.

FIGURE -5
NORMALIZED SHORT-CIRCUIT CURRENT VS. $\frac{W}{L_p}$

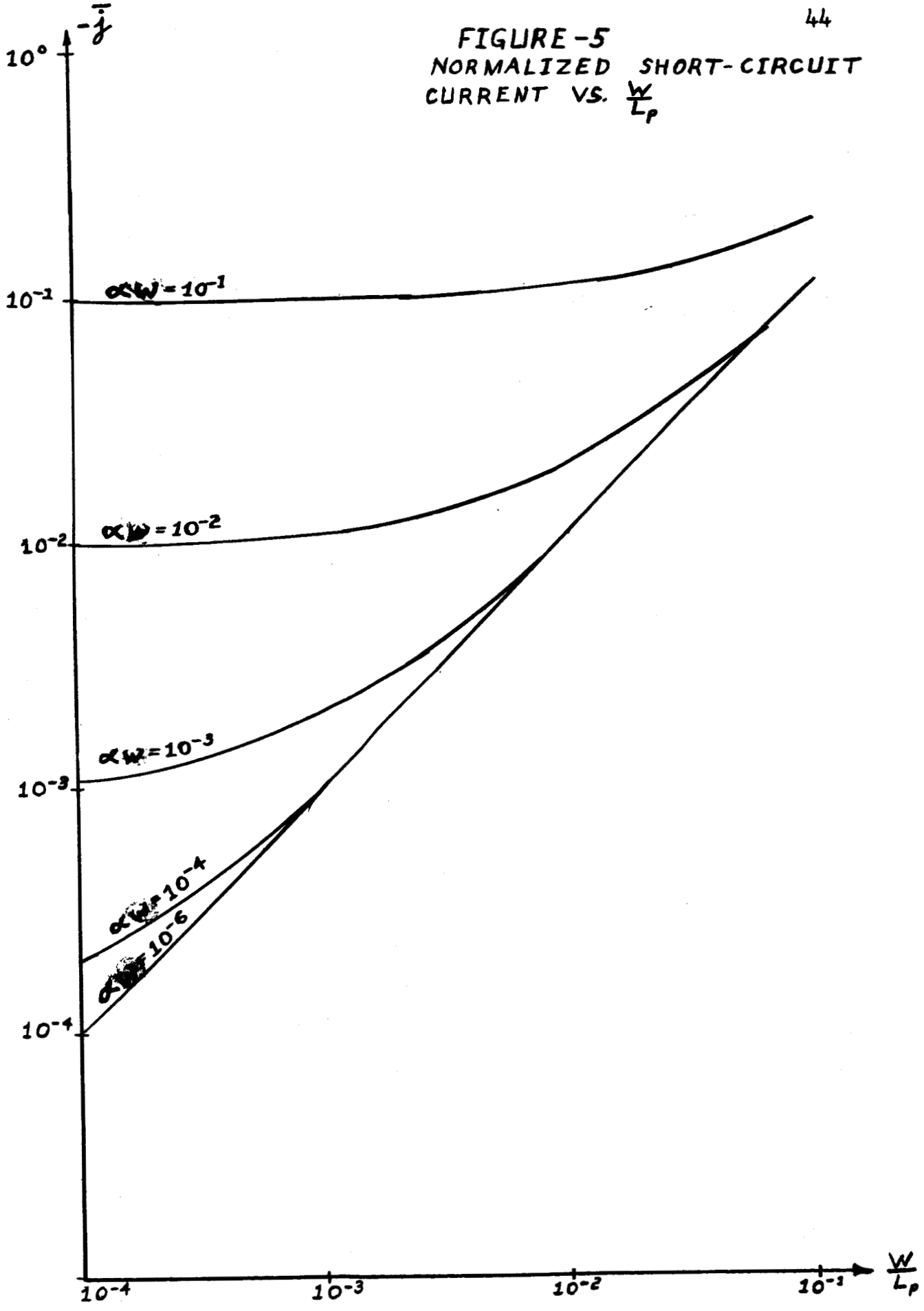

FIGURE - 6
NORMALIZED SHORT-CIRCUIT CURRENT, $\bar{J}$, VS S'/W
$\frac{W}{L_p} = 10^{-2}$

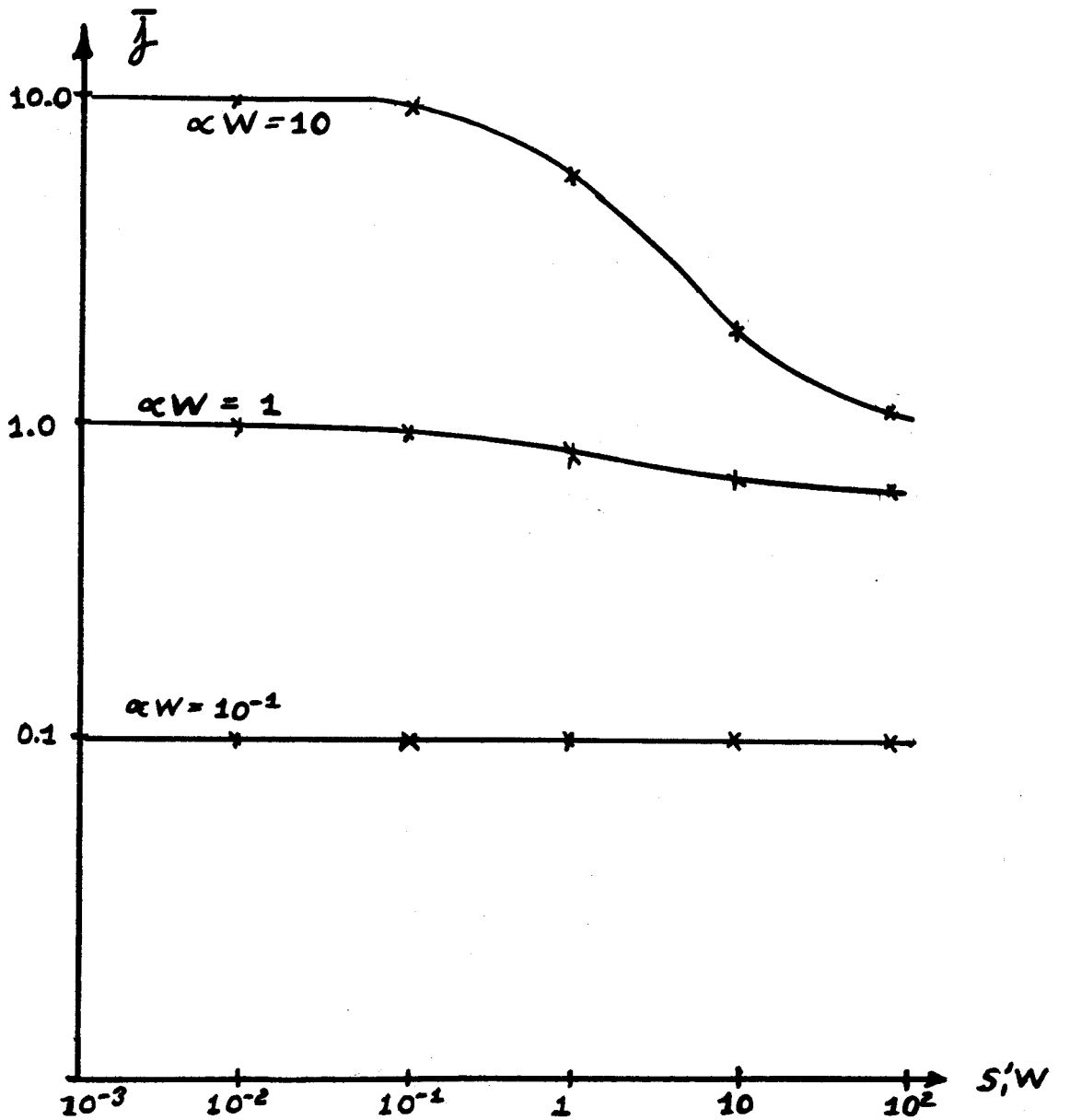

IV. Projected Plans

In the area of filament studies, additional gamma data will be taken especially for surfaces passivated with silicon oxide. Modeling for the gamma damage has already begun and should be completed in the next three months. X-radiation studies on passivated and non-passivated surfaces should begin during the summer of this year (1965). Proton irradiation studies will probably take place during the latter months of this grant year.

Now that successful "pin hole free" oxide growths have been obtained, devices of the M. O. S. type will be fabricated and charge and surface potential data obtained for various radiation ambients. Gamma, x- and possibly proton fields will be considered. Computer tabulations of the important surface theories are nearing completion.

The analysis phase of this work will continue during the whole of the second grant year. Two and three-dimensional modeling of the bipolar planar transistor will follow the solar cell studies with emphasis placed on surface parameter effects.

It is believed that the data shown here, along with data which will be gathered in the future are worthy of publication and it is expected that several manuscripts will be prepared during the next few months and submitted to appropriate research journals.

V. Appendix A

One may write Poissons equation for a positive charge as

$$\frac{\partial^2 \phi}{\partial x^2} = -\frac{\rho}{\epsilon_r \epsilon_0} \tag{1}$$

where is the difference between the electrochemical and electrostatic potentials in the crystal and is positive for n-type material. However

$$\rho = q(p - n + N_D^+ - N_A^-) \tag{2}$$

the assumption is made here that all donors and acceptors are ionized. In the bulk where charge neutrality prevails, we know that

$$p_0 - n_0 = N_A^- - N_D^+ \tag{3}$$

where

$$n_0 = n_i e^{\frac{q\phi_B}{kT}} \tag{4}$$

and

$$p_0 = n_i e^{-\frac{q\phi_B}{kT}} \tag{5}$$

assuming non-degeneracy.

Thus

$$p_0 - n_0 = N_A^- - N_D^+ = -2n_i \sinh \frac{q\phi_B}{kT} \tag{6}$$

and

$$p - n = -2n_i \sinh \frac{q\phi}{kT} \tag{7}$$

Thus equation (1) becomes

$$\frac{\partial^2 \phi}{\partial x^2} = -\frac{2n_i q}{\epsilon_r \epsilon_0}\left(\sinh \frac{q\phi_B}{kT} - \sinh \frac{q\phi}{kT}\right) \tag{8}$$

If we now let $\frac{q\phi}{kT} = u$ and $L_D = \left(\frac{\epsilon_r \epsilon_0 kT}{2q^2 n_i}\right)^{1/2}$

the above equation becomes

$$\frac{\partial^2 \phi}{\partial x^2} = \frac{1}{L_D^2}\left(\sinh u - \sinh u_B\right) \tag{9}$$

Upon integrating once between $u = u_B$ and $u = u$ one gets

$$\frac{\partial \phi}{\partial x} = \pm \frac{\sqrt{2}}{L_D}\left[\sinh u_B(u_B - u) - (\cosh u_B - \cosh u)\right]^{1/2} \tag{10}$$

If we let

$$F(u, u_B) = \sqrt{2}\left[\sinh u_B(u_B - u) - (\cosh u_B - \cosh u)\right]^{1/2}$$

we can write an expression for the $\bar{E}$ field at the surface as

$$E_s = -\left(\frac{\partial \Phi}{\partial x}\right) = \left(\frac{kT}{q L_D}\right) F(u_s, u_B)$$

Papers by C. E. Young[4] and R. H. Kingston and S. F. Neustalter[5] contain curves as a graphical representation of this function but due to the size of the curves the very important minimum in the ΔG vs Q_s curves can not be well defined. For this reason a computer program was set up and $F(u, u_B)$ was calculated for u_s from +20 to -20 and u_B from +20 to -20. A $G(u, u_B)$ function was also calculated on the computer for the same range on both u_B and u_s. The G function allows one to calculate $\Delta\sigma$ as a function of surface potential.[6]

Since electron and hole excesses are

$$\Gamma_n = \int_0^\infty (\bar{n} - n_B)\, dx$$

$$\Gamma_p = \int_0^\infty (\bar{p} - p_B)\, dx$$

and since $$dx = \frac{dx}{du} du = \frac{L_D}{F(u, u_B)} du$$

then $$\Delta n = \Gamma_n = n_i L_D \int_{u_s}^{u_B} \frac{e^u - e^{u_B}}{F(u, u_B)} du = n_i L_D G(-u_s, -u_B)$$

and similarly $$\Delta p = \Gamma_p = n_i L_D\, G(u_s, u_B)$$

Having this we can write

$$\Delta\sigma = q \mu_p [\Delta p + b \Delta n]$$

$$\Delta\sigma = q \mu_p n_i L_D [G(u_s, u_B) + b\, G(-u_s, -u_B)]$$

which is the change in conductance as a function of surface potential.

VI. Bibliography

1. Blakemore, J., Semiconductor Statistics, pp. 269-277, Pergamon Press, New York, N. Y., 1962.
2. Atalla, M. M., Tannenbaum, E., and Scheibner, E. J., Bell System Technical Journal, Vol. 38, pp. 749-783, 1959.
3. Brown, W. L., Physical Review, Vol. 100, pp. 590-591, 1955.
4. Young, C. E., Journal of Applied Physics, Vol. 32, pp. 329-332, 1961.
5. Kingston, R. H., and Neustaiter, S. F., Journal of Applied Physics, Vol. 26, pp. 718-720, 1955.
6. Levine, S. N., Principles of Solid State Microelectronics, Holt, Rinehart and Winston, New York, N. Y., 1963.